







TDP-43 stabilizes G3BP1 mRNA: relevance to amyotrophic lateral sclerosis/frontotemporal dementia

Hadjara Sidibé,^{1,2} Yousra Khalfallah,^{2,3} Shangxi Xiao,⁴ Nicolás B. Gómez,^{5,6} Hana Fakim,^{1,2} Elizabeth M. H. Tank,⁵ Geneviève Di Tomasso,³ Eric Bareke,² Anaïs Aulas,^{2,3}  Paul M. McKeever,⁴ Ze'ev Melamed,⁷ Laurie Destroimaisons,² Jade-Emmanuelle Deshaies,² Lorne Zinman,⁸ J. Alex Parker,^{1,2}  Pascale Legault,³ Martine Tétrault,^{1,2}  Sami J. Barmada,^{5,6,9} Janice Robertson⁴ and  Christine Vande Velde^{1,2}

TDP-43 nuclear depletion and concurrent cytoplasmic accumulation in vulnerable neurons is a hallmark feature of progressive neurodegenerative proteinopathies such as amyotrophic lateral sclerosis (ALS) and frontotemporal dementia (FTD). Cellular stress signalling and stress granule dynamics are now recognized to play a role in ALS/FTD pathogenesis. Defective stress granule assembly is associated with increased cellular vulnerability and death. Ras-GAP SH3-domain-binding protein 1 (G3BP1) is a critical stress granule assembly factor.

Here, we define that TDP-43 stabilizes G3BP1 transcripts via direct binding of a highly conserved cis regulatory element within the 3' untranslated region. Moreover, we show *in vitro* and *in vivo* that nuclear TDP-43 depletion is sufficient to reduce G3BP1 protein levels. Finally, we establish that G3BP1 transcripts are reduced in ALS/FTD patient neurons bearing TDP-43 cytoplasmic inclusions/nuclear depletion.

Thus, our data indicate that, in ALS/FTD, there is a compromised stress granule response in disease-affected neurons due to impaired G3BP1 mRNA stability caused by TDP-43 nuclear depletion. These data implicate TDP-43 and G3BP1 loss of function as contributors to disease.

1 Department of Neurosciences, Université de Montréal, Montréal, QC H3A 0E8, Canada

2 CHUM Research Center, Montréal, QC H2X 0A9, Canada

3 Department of Biochemistry, Université de Montréal, Montréal, QC H3A 0E8, Canada

4 Tanz Centre for Research in Neurodegenerative Diseases, University of Toronto, Toronto, ON M5T 0S8, Canada

5 Department of Neurology, University of Michigan, Ann Arbor, MI 48109, USA

6 Cellular and Molecular Biology Program, University of Michigan, Ann Arbor, MI 48109, USA

7 University of California, San Diego/Ludwig Institute for Cancer Research, San Diego, CA 92093, USA

8 Division of Neurology, Department of Medicine, Sunnybrook Health Sciences Centre, University of Toronto, Toronto, ON M4N 3M5, Canada

9 Neuroscience Graduate Program, University of Michigan, Ann Arbor, MI 48109, USA

Correspondence to: Christine Vande Velde, PhD

Department of Neurosciences, Université de Montréal, CRCHUM-Tour Viger

900, Rue Saint-Denis, R09.474, Montréal, QC H2X 0A9, Canada

E-mail: c.vande.velde@umontreal.ca

Keywords: TDP-43; amyotrophic lateral sclerosis; frontotemporal dementia; G3BP1; stress granules

Received September 15, 2020. Revised March 26, 2021. Accepted May 27, 2021. Advance access publication June 11, 2021

© The Author(s) (2021). Published by Oxford University Press on behalf of the Guarantors of Brain.

This is an Open Access article distributed under the terms of the Creative Commons Attribution-NonCommercial License (<https://creativecommons.org/licenses/by-nc/4.0/>), which permits non-commercial re-use, distribution, and reproduction in any medium, provided the original work is properly cited. For commercial re-use, please contact journals.permissions@oup.com

Abbreviations: ALS = amyotrophic lateral sclerosis; FTD = frontotemporal dementia; FTLN = frontotemporal lobar degeneration; smFISH = single molecule fluorescent *in situ* hybridization; UTR = untranslated region

Introduction

TDP-43 is a ubiquitously expressed, mainly nuclear, RNA/DNA binding protein belonging to the heterogeneous nuclear ribonucleoprotein family (hnRNPs). It is a major regulator of RNA metabolism and is involved in several steps of RNA regulation (mRNA transport, nucleocytoplasmic export, stability, transcription, translation, splicing, etc.).¹ Like other hnRNPs, TDP-43 has an N-terminal domain containing a nuclear localization sequence (NLS), an RNA-binding domain (RBD) composed of two RNA recognition motifs (RRM1 and RRM2) and a glycine rich C-terminal domain, containing intrinsically disordered regions.¹ While the NLS dictates the localization of TDP-43 to the nucleus, the RRMs are essential for specific interaction with target RNAs, and the N- and C-terminal domains serve as platforms to mediate TDP-43 self-assembly and interaction with other protein partners, respectively.^{2–4}

TDP-43 proteinopathies refer to a group of neurological disorders characterized by the pathological accumulation of TDP-43 in the cytoplasm of affected neurons and, less frequently, oligodendroglia.⁵ The fatal neurodegenerative diseases amyotrophic lateral sclerosis (ALS) and frontotemporal dementia (FTD) are included in this group. FTD, the second most common cause of dementia in those <65 years, is caused by the degeneration of the frontal and temporal lobes (referred to as frontotemporal lobar degeneration or FTLN). ALS shares clinical, neuropathological and genetic overlaps with FTD. In addition to the neuromuscular component of ALS, ~50% of ALS patients exhibit cognitive impairment caused by FTLN, with 15% fulfilling the clinical diagnostic criteria of FTD.⁶ TDP-43 nuclear depletion and concomitant accumulation in the cytoplasm, often phosphorylated and as a component of skein-like or round inclusions, in motor and cortical neurons is observed in 97% of all ALS cases and 50% of patients with FTD.¹ Given these shared clinical and pathological features, ALS and FTD with TDP-43 pathology are now considered to be part of the same disease spectrum.¹ However, it remains debated as to whether nuclear depletion of TDP-43 with simultaneous cytoplasmic accumulation, which may be of another conformation, induces a loss or gain of function effect, or some combination thereof.

The interplay between genetics and the environment is suspected to play a major role in the development and/or progression of ALS and FTD.⁷ Recent work places stress granules, a core aspect of the integrated stress response that facilitates cellular recovery from adverse environmental exposures, as a critical component of disease pathogenesis.^{8–11} These micrometre-sized cytoplasmic foci form concomitant with translational arrest following stress exposure and are proposed to protect and/or sort non-translating mRNAs.^{12,13} The key protein for stress granule assembly is G3BP1 (Ras-GAP SH3-domain-binding protein 1).^{14,15} We have previously demonstrated that G3BP1 protein and transcript levels are decreased as TDP-43 levels are lowered, which compromises cellular viability post-stress.^{16–19} This TDP-43-induced G3BP1 depletion disrupts stress granule dynamics, which can be rescued by the reintroduction of G3BP1.¹⁸ Recent work reinforces that G3BP1 is central to stress granule formation as it is a tuneable switch regulating the liquid–liquid phase separation (LLPS) required for stress granule formation.^{16,18,20–22} Thus, we reason that defining the

molecular mechanism underlying TDP-43 modulation of G3BP1 is essential to understanding the contribution of stress granule biology to ALS and FTD pathogenesis.

Herein, we demonstrate that nuclear TDP-43 depletion, as observed in the neurons of ALS/FTD patients, as well as expression of pathological TDP-43 variants associated with ALS/FTD, impact G3BP1 mRNA metabolism. Additionally, we have uncovered that while there are two G3BP1 transcripts encoding the same protein, only one of them is regulated by TDP-43. TDP-43 binds and stabilizes the short G3BP1 transcript via an evolutionary conserved sequence. Finally, we demonstrate that this transcript is the predominant transcript expressed in adult human motor neurons and G3BP1 mRNA is decreased in ALS/FTD patient neurons featuring TDP-43 nuclear depletion/cytoplasmic aggregation. Taken together, our work suggests that compromised stress granule assembly due to the loss of TDP-43 nuclear function in G3BP1 stability may be relevant to disease pathogenesis.

Materials and methods

Constructs

Flag-TDP-43^{ΔNLS} (siRNA-resistant) was generated using the QuickChange® II Site-Directed mutagenesis kit (Agilent Technologies) on pCS2-Flag-TDP-43-WT²³ with the forward primer 5'-CAACTATCCAAAAGATAACGCAGCAGCAATGGATGAGACAGATGC-3' and its complementary reverse to mutate the NLS, as previously published.²⁴ Modifications to render TDP-43 plasmids siRNA-resistant were performed with the forward primer 5'-CTTCCTAATTCTAAGCAGAGGCAGGACGAGCCTTTGAGAAGC-3' and its complementary reverse. The His-G3BP1cDNA-3' untranslated region (UTR) construct was subcloned into pTRE-tight, which was provided by Dr Yves Berthiaume (Institut de recherche cliniques de Montréal). His-G3BP1 was generated by PCR with the forward primer coding for His-tag: forward 5'-CTAGGATCCGCAATGC ACCACCACC ACCACCACGTGATGGAGAA GCCTAGTCCCCTG-3'; reverse 5'-ATCGCAGCTAGCGCACCTGCCGTGGCGCAAGC-3' and inserted using BamHI and NheI restriction sites. G3BP1 3' UTR was generated using PCR amplification with the following primers: forward 5'-ATCGCAGCTAGCGCGTGAATCTTCATGGATCTTCATGCAG-3' and reverse 5'-GCCTAATCGATGCAAACAAAACCTTCACCCATCTCAC-3' and inserted using NheI and ClaI restriction sites. Deletion of nucleotides (nt) 319–372 (GRCh38/hg38 chr5:151804204–151804257) was made using the following phosphorylated primers: forward 5'-5'/phos/CTTAAGCAGTTTATAACAGACTGGGGTCATA-3' and reverse 5'-5'/phos/CCTGACCTTTAGTCTTTCACCTTCCAATTTTG-3'.

Cell culture and transfection

HeLa, human embryonic kidney 283 (HEK293), U2OS and Mo3.13 cells were cultured in Dulbecco's high glucose modified Eagle medium (DMEM, GE Healthcare) supplemented with 10% foetal bovine serum (FBS, Wisent) and 2 mM L-glutamine (Sigma). HeLa Tet-off cells were cultured in DMEM supplemented with 10% tetracycline-free FBS (Wisent) and 2 mM L-glutamine. SH-SY5Y and SK-N-SH cells were cultured in Dulbecco's high glucose modified Eagle

medium/Nutrient Mixture F-12 Ham (DMEM-F12, ThermoFisher Scientific) supplemented with 10% FBS (Gibco), 2 mM L-glutamine and 1% MEM non-essential amino acids (ThermoFisher Scientific). Cells were collected 72 h after transfection with 125 pmol Stealth siRNA using Lipofectamine[®] 2000 (Invitrogen) and 24 h after plasmid transfection using Lipofectamine LTX and Plus reagent (Invitrogen). The siRNA sequences used were: Control (siCTL): no. 12935-200 (Invitrogen), and TDP-43 (siTDP-43): 5'-AAGCAAAGCCAA GAUGAGCCUUUGA-3', as previously published.^{16–18,25}

Human neuron differentiation

Human induced pluripotent stem cells (iPSCs) from a healthy 54-year-old female were reprogrammed from fibroblasts via transfection with episomal vectors encoding seven reprogramming factors, as previously described.^{26,27} A polycistronic construct containing a doxycycline-inducible cassette driving expression of the transcription factors neurogenins 1 and 2,^{28,29} Dendra2-tagged TDP-43 (wild-type or M337V) and eIF3-iRFP was integrated into the *CLYBL* safe harbour locus on chromosome 13. For creation of TDP-43(M337V), the homologous recombination vector used to insert Dendra2 was modified to include the corresponding mutation in the *TARDBP* open reading frame (c.1009A>G). All insertions and base pair mutations were verified by PCR and Sanger sequencing. As described in previous work,^{30,31} integration of this cassette enables rapid, robust and consistent differentiations and produces homogenous cultures of forebrain-like, excitatory, glutamatergic neurons optimal for subsequent biochemical or genetic studies.³² Cells were collected in TRIzol[®] at day *in vitro* 10. Lines are verified mycoplasma-free on a monthly basis.

Immunoblotting

Proteins were extracted with RIPA buffer (150 mM NaCl, 50 mM Tris pH 7.4, 1% Triton[™] X-100, 0.1% SDS, 1% sodium deoxycholate) with protease inhibitors (10 µg/ml leupeptin, 10 µg/ml pepstatin A, 10 µg/ml chymostatin), separated by SDS-PAGE, transferred to nitrocellulose and blocked with 5% powdered milk in PBS-T (137 mM NaCl, 2.7 mM KCl, 8 mM Na₂HPO₄, 1.5 mM KH₂PO₄, 1% Tween-20). Membranes were incubated with rabbit anti-TDP-43 (10789-2-AP; Proteintech), mouse anti-Actin (69100; MP Biomedicals) and mouse anti-G3BP1 (sc-81940; Santa Cruz) followed by HRP-conjugated secondary antibodies (Jackson ImmunoResearch) and labelled with ECL chemoluminescence (ThermoFisher Scientific). Films were quantified by densitometry using Photoshop (Adobe, CS4).

Immunofluorescence

Coverslips were fixed in 1% formaldehyde/PBS, washed with PBS, permeabilized in 0.1% Triton[™] X-100/PBS and blocked in 0.1% bovine serum albumin (BSA)/PBS. Coverslips were incubated with primary antibodies: mouse anti-Flag (F1804; Sigma) and rabbit anti-TDP-43 (10789-2-AP; Proteintech) diluted in 0.1% BSA/PBS; washed once with 0.1% Triton[™] X-100/PBS and then twice with 0.1% BSA/PBS. Coverslips were then incubated with secondary antibodies: donkey anti-mouse Alexa 488 (Jackson ImmunoResearch) and donkey anti-rabbit Alexa 594 (Jackson ImmunoResearch) diluted in 0.1% BSA/PBS, washed, labelled with TO-PRO[™]-3 iodide (ThermoFisher Scientific) and mounted using ProLong[™] Antifade (ThermoFisher Scientific). Images were collected on a Leica TCS SP5 confocal microscope equipped with 40× (1.25 numerical aperture) oil objective and the Leica Application Suite imaging software.

Single molecule fluorescent *in situ* hybridization

Custom DNA probe sets (20mers) were designed using Stellaris[®] Probe Designer for total G3BP1 (targeting the G3BP1 open reading frame and a portion of the 3' UTR) and the long G3BP1 (targeting a unique region in the long G3BP1 3' UTR) (Supplementary Table 1). Probes were purchased from Biosearch Technologies, with the total G3BP1 probes labelled with Quasar 570 and long G3BP1 probes labelled with Quasar 670. For single molecule fluorescent *in situ* hybridization (smFISH), the protocol was adapted from Rahman *et al.*³³ Briefly, HeLa cells were plated on glass coverslips and treated with control or TDP-43 siRNA (see previously). Coverslips were then washed with 1× PBS, fixed with 4% paraformaldehyde (PFA) for 10 min at room temperature, washed twice with wash buffer (10% formamide, 2× SSC) and stored overnight in 70% ethanol at –20°C. Cells were washed in wash buffer and then hybridized with 125 nM of each probe set (total and long) with 40 µg of ssDNA/tRNA resuspended in hybridization buffer (10% dextran sulphate, 10% formamide, 2× SSC, 2 mM vanadyl ribonucleoside complexes, 0.1 mg/ml BSA) for 3 h in the dark at 37°C in a humid hybridization chamber. Cells were then washed twice with wash buffer at 37°C for 30 min each. The second wash was supplemented with 1:10 000 Hoechst. Cells were washed twice with 1× PBS and mounted with ProLong[™] Gold antifade reagent. Images were acquired using a confocal Leica TCS_SP5 MP microscope at 63× oil (×1.5 zoom) objective and using a single z-plane focused on the channel for nuclear Hoechst. At least three to five frames were captured per condition and repeated for three biological replicates. Fifteen cells were counted per experiment for each condition using ImageJ/FIJI. The *Region of Interest* tool was used to draw the boundary of each cell and foci per cell were counted for each channel using the *Find maxima* tool at >80 prominence to generate a mask of foci. A nuclear mask was generated in the Hoechst channel by adjusting the threshold. Co-localization between magenta and green foci, and the nucleus, were calculated using the masks generated and the Object based methods in the JACoP plugin in ImageJ.³⁴ Foci were plotted using Prism and statistical analysis was performed using an unpaired t-test with the Welch correction.

Cell line reverse transcription quantitative PCR

RNA was extracted using RNeasy[®] Minikit (Qiagen) and treated with DNase I (Qiagen) according to the manufacturer's instructions. Equal amounts of RNA were reverse transcribed using the QuantiTect Reverse Transcription kit (Qiagen). The QuantiStudio 7 Flex Real-Time PCR System (Life Technologies) was used for quantitative PCR (qPCR). PrimeTime Standard qPCR assays (IDT) were: GAPDH (targeting exons 1–2) Hs.PT.39a.22214836; G3BP1 total (targeting exons 6 and 7) Hs.PT.58.20396264; G3BP1 long forward: 5'-TCTTACTGGACACTCAACCTTG-3'; G3BP1 long reverse: 5'-TGCCATAACTTTTGTGACTTCATG-3'; G3BP1 long detection probe 5'-56-FAM/AGCTTCCCC/Zen/AGTGCTTTCTGTGCAT/3IABkFQ-3' 18S forward: 5'-CCAGTAAAGTGGGTGTCATAAG-3'; 18S reverse: 5'-GGCCTCACTAAACATCCAA-3'; 18S detection probe 5'-56-FAM/TGCGTTGAT/Zen/TAAGTCCCTGCCCTT/3IABkFQ-3'. Data were analysed using the 2^{–ΔΔCT} method. The genes of interest were standardized to the geometric mean of two housekeeping genes (GAPDH and 18S).

RNA immunoprecipitation

HeLa cells were lysed in 50 mM Tris, pH 7.5, 150 mM NaCl, 0.5% NP-40, 1 mM MgCl₂, with protease inhibitors and RNase inhibitors,

trituated subsequently through 18G and 25G needle syringes, incubated for 30 min at room temperature, centrifuged at 13 000g and the supernatant collected. Aliquots of 10 mg of precleared lysate were immunoprecipitated at 4°C for 6 h with rabbit anti-TDP-43 (10789-2-AP; Proteintech) or rabbit anti-Flag as control IgG (F1804; Sigma) prebound to Protein G Dynabeads™ (ThermoFisher Scientific). Immunoprecipitates were treated with DNase (Qiagen) and RNA was recovered with TRIzol® (Invitrogen) and chloroform (Fisher Scientific). Equal amounts of RNA were reverse transcribed using the QuantiTect Reverse Transcription kit (Qiagen). Standard PCR was used to amplify cDNA with the following primers: total G3BP1 forward 5'-AAGCCCTTCCACTCCAA-3'; total G3BP1 reverse 5'-TAATCGCCTTCGGGGACCTG-3' (targeting exon 12); long G3BP1 forward 5'-CACTGAGGTCTCCCGATA-3'; long G3BP1 reverse 5'-CCAGACCAATGGAAGCACT-3'; CAMKII forward 5'-CCACAGGGCTTTAGGAGA-3'; CAMKII reverse 5'-GCTGCTGCCGCTTTTGTGA-3'; HSPA1A forward 5'-TGAAGGAGACAGCCGAAAG-3'; HSPA1A reverse 5'-TGCATCAGTATAGAAAACAAGAA-3'.

Luciferase assays

HeLa cells were transfected with siRNA for 48 h, and then subsequently transfected using FuGENE® (Promega) for 24 h with reporter plasmids including the promoter and 3' UTR of human G3BP1 (SwitchGear Genomics) and relevant controls, as recommended by the manufacturer (for the promoter assay: GAPDH and a vector containing random sequence, R01; for 3' UTR: GAPDH, HDAC6 and vector containing random sequence, R03). The LightSwitch Assay (Promega) reagents were added according to the manufacturer's instructions and luciferase activity was assessed with a Synergy H4 Hybrid Multi-Mode Microplate reader (Biotek).

RNA stability assay

HeLa Tet-off cells were subjected to siRNA using Lipofectamine® 2000 (Invitrogen) for 48 h then transfected for 24 h with 1 µg of His-G3BP1 3' UTR constructs using Lipofectamine® LTX and Plus reagent (Invitrogen). To determine mRNA stability, HeLa cells were treated with 1 µg/ml doxycycline (Sigma) for 0.5, 1, 1.5, 2, 4 or 6 h before RNA extraction with the RNeasy® Minikit (Qiagen). Equal amounts were reverse transcribed via the QuantiTect Reverse Transcription kit (Qiagen), according to the manufacturer's instructions. The QuantStudio 7 Flex Real-Time PCR System (Life Technologies) was used for qPCR. PrimeTime Standard qPCR assays (IDT) for His-G3BP1 forward 5'-ACGTGATGGAGAAGCCTAGT-3'; His-G3BP1 reverse 5'-TGACATCACTTCTCTGTGGATTT-3'; His-G3BP1 detection probe 5'-56-FAM/CGGGCGGGGA/Zen/ATTTGTGAGACAGTA/3IABkFQ-3'; 18S forward 5'-CCAGTAAAGTGGGGTCATAAAG-3'; 18S reverse 5'-GGCCTCACTAAACCATCCAA-3'; 18S detection probe 5'-56-FAM/TGCGTTGAT/Zen/TAAGTCCTGCCCTT/3IABkFQ-3'.

Caenorhabditis elegans reverse transcription quantitative PCR

Some strains were provided by the CGC, which is funded by NIH Office of Research Infrastructure Programs (P40 OD010440). RNA from N2 and *tdp-1(ok803)* strains was extracted using TRIzol® (Invitrogen) and chloroform (Fisher Scientific). Equal amounts of RNA were reverse transcribed using the QuantiTect Reverse Transcription kit (Qiagen). The cDNA was amplified with the following primer sets: *ama-1*: Ce02462726_m1 (targeting exon boundary 12–13), *gtbp-1*: Ce02458711_g1 (targeting exon boundary 5-6).

RNA pull down

Lysates were prepared in pulldown buffer (10 mM Tris pH 7.4, 50 mM NaCl, 0.5% Triton™ X-100) with protease inhibitors (10 µg/ml leupeptin, 10 µg/ml pepstatin A, 10 µg/ml chymostatin) and subsequently trituated with a 25G needle. Protein G Dynabeads™ (ThermoFisher) were prepared according to the manufacturer's instructions. Then 100 µg of lysates or 100 ng of TDP-43 recombinant protein (NM_007375, OriGene) were incubated with 30 pmol of biotin-labelled RNA for 1 h at 4°C. Proteins were eluted with 2.5 × Laemmli buffer and immediately analysed by immunoblotting with rabbit anti-TDP-43 (10789-2-AP; Proteintech) and rabbit anti-hnRNP L (156682; Abcam). Probes: positive control GRN (nt262-288): biotin-UGUGUGUGUGUGCGGUGUGUGUGUGUG; negative control (AC)₁₂: biotin-ACACACACACACACACACACACACACAC; G3BP1 (nt334-358): biotin-UUUUUUGUGUGUUAUGGUGUGUGUG.

Recombinant protein expression and purification

The RRM1 and RRM2 domains of TDP-43 (amino acids 102–269) in the wild-type and F147L/F149L mutant forms were subcloned from the pCS2 vector²³ to the pET21b vector (Novagen) modified to include a tobacco etch virus cleavage site, and the resulting plasmids were transformed into *Escherichia coli* host strain BL21 (DE3). The bacteria were grown at 37°C in Luria-Bertani media, and protein expression was induced with 1 mM isopropyl-β-D-1-galactopyranoside (IPTG) for 4 h at 30°C. The cells were collected by centrifugation and resuspended in lysis buffer (25 mM HEPES pH 8.0, 500 mM NaCl, 1 mM DTT) supplemented with 0.15% (w/v) Protease Inhibitor Cocktail (Sigma-Aldrich). The cells were lysed by French press, sonicated for 10 s and centrifuged at 11 000g for 30 min at 4°C. The supernatant was incubated at 4°C for 1 h with Ni-charged IMAC Sepharose™ 6 Fast Flow (GE Healthcare). The resin was then washed three times with His-A buffer (lysis buffer + 20 mM imidazole). The bound His₆-tagged TDP-43₁₀₂₋₂₆₉ fusion protein was eluted from the washed resin by two 10-min incubations at room temperature with His-B buffer (lysis buffer + 30 mM imidazole) followed by centrifugation. The supernatant containing the protein of interest was dialysed overnight at 4°C in FPLC-A buffer (25 mM HEPES pH 8.0, 100 mM NaCl, 1 mM DTT) supplemented with tobacco etch virus protease (kindly provided by J. G. Omichinski, Université de Montréal). The retentate was then applied to a Q Sepharose High-Performance column (GE Healthcare; 60-ml bed volume) equilibrated with FPLC-A buffer. The protein was eluted from the column using a gradient (from 0% to 50% over 450 ml) of FPLC-B buffer (FPLC-A + 1 M NaCl). The pooled fractions containing the protein of interest were dialysed overnight at 4°C in storage buffer (25 mM HEPES pH 8.0, 100 mM NaCl, 2 mM DTT and 20% glycerol) and the protein was stored at -80°C. The purity of the protein (>98%) was assessed by Coomassie-stained SDS-PAGE.

RNA preparation

The TDP-43 binding sequence of human G3BP1 3'-UTR (G3BP1-RNA₃₂: 5'-TTGTGTGTTAAATGGTGTGTGCTCCCTCTCCA-3') was first cloned into the pARiBo4 plasmid.³⁵ After plasmid linearization with EcoRI, the ARiBo-fusion RNA was *in vitro* transcribed for 3 h at 37°C using standard conditions.³⁵ The RNA was then purified using the ARiBo affinity purification method under non-denaturing condition,³⁶ as previously described.³⁵ The purified RNA was concentrated with Amicon Ultra-4 centrifugal filter devices (Millipore), and exchanged in H₂O. For radioactive labelling of the RNA, an alkaline phosphatase treatment was first performed for 1 h at 37°C, followed by inactivation of the enzyme at 65°C for 15 min. The RNA was then 5' end-labelled with γ-(³²P) ATP (PerkinElmer) using T4 polynucleotide kinase (New England Biolabs) according to the manufacturer's instructions and then further

purified by 15% denaturing gel electrophoresis. After gel extraction, the ^{32}P -labelled RNA was resuspended in TE buffer (10 mM Tris pH 7.6, 1 mM EDTA) and stored at -20°C .

Electrophoretic mobility shift assay

The ^{32}P -labelled RNA was first refolded by heating 2 min at 95°C and snap-cooling on ice for 5 min. The protein samples were diluted in electrophoretic mobility shift assay (EMSA) buffer (50 mM Tris pH 7.5, 50 mM NaCl, 0.05% NP40, 2 mM DTT and 20% glycerol), and the concentrations were adjusted to span from $0.01\times$ to $5\times$ of the estimated dissociation constant, K_d . The binding reactions (20 μl) were initiated by mixing 10 pM of ^{32}P -labelled RNA with the diluted protein and incubating at 4°C for 30 min. For each K_d determination, binding reactions were loaded on a 10% native polyacrylamide gel (37.5:1 polyacrylamide/bisacrylamide) and run in Tris-Glycine buffer (25 mM Tris-base, 200 mM glycine) at 200 V for 2 h, with active water cooling in a cold room. The gels were then dried and exposed overnight to a storage phosphor screen. The ^{32}P -labelled RNA was visualized with a Bio-Rad Personal Molecular Imager and band intensities were quantified using the ImageLab software (v.5.2.1, Bio-Rad). The fraction of bound RNA was plotted against protein concentration, and the data fitted to the Hill equation by non-linear regression analysis within the OriginPro 2015 software (OriginLab). Four independent K_d determination experiments were performed for the wild-type TDP-43¹⁰²⁻²⁶⁹. The reported K_d reflects the average values and the standard deviations from these multiple experiments.

Sciatic axotomy and immunofluorescence

The use of animals and all procedures were performed according to the guidelines of the Canadian Council on Animal Care and were approved by the CRCHUM Institutional Committee for the Protection of Animals. Female C57BL/6 mice (6–8 weeks, $\sim 20\text{g}$) were purchased from Charles River Laboratories. Our experiments were based on a previously published protocol for axotomy³⁷ with modifications. Mice were weighed and anaesthetized by exposure to 1.5 l/min oxygen and 4% isoflurane. After loss of limb reflexes, animals were transferred to a mask system and maintained with 1 l/min oxygen and 2% isoflurane. For a medial axotomy, mice were shaved and the site of surgery sterilized. The right sciatic nerve was exposed with an incision 1 cm below the exit from the pelvic bone. The nerve was then cut 1 cm distal from the exit point of spinal nerve roots. A surgical sterile sponge soaked in 5% Fluoro-Gold (Fluorochrome, LLC) in sterile saline was deposit at the site of the nerve cut to enable visualization of injured motor neurons post-injury. Mice were allowed to recover in a clean heated cage and allowed free access to food and water. Pain was managed with buprenorphine injection just prior to surgery, followed by a slow-release formulation injected 5 h post-surgery. Neurobehavioural assessments based on a previously published scale^{37,38} were conducted at Days 1, 3, 5 and 7 post-injury. Following transcardiac perfusion with saline and 4% PFA, tissues were cryopreserved and subsequently sectioned, then permeabilized and blocked with 0.5% Tween-20 and 5% normal donkey serum (Jackson ImmunoResearch, 017-000-121) for 45 min at room temperature. Primary antibody incubations were performed in 0.3% Tween-20 in PBS overnight at 4°C , followed by an appropriate fluorescently conjugated secondary antibodies against the desired species (Jackson ImmunoResearch). Antibodies used were mouse anti-TDP-43 (1:500, R&D, MAB7778), rabbit anti-G3BP1 (1:4500, Proteintech, 13057-2-AP) and guinea pig anti-FluoroGold (1:750, NM-101 FluGgp, Protos Biotech Corp.). Images were collected using a confocal microscope (SP5; Leica) equipped with LAS

AF software (Leica) for acquisition at $\times 63$. Adobe Photoshop CC 2018 was used for quantification of fluorescence intensity. A line was drawn across and the longest axis of the neuron and the highest intensity along that line was recorded. This maximum intensity of a FluoroGold-positive neuron was expressed relative to the maximum intensity mean of 10 FluoroGold-negative neurons. In total, 30 neurons (10 neurons from three mice each) were quantified. Importantly, all compared images were acquired with the same microscope settings.

RNAscope and immunofluorescence on patient autopsy material

Autopsy tissues from ALS and ALS/FTLD cases were collected in accordance with the local ethics review board at Sunnybrook Health Sciences Centre, Toronto. Orbitofrontal cortex (Brodmann areas 11 and 47) from four sporadic ALS cases with FTLD, as assessed by presence of TDP-43 pathology (ALS/FTLD-TDP-43), and four sporadic ALS cases without FTLD were used for the study (Supplementary Table 2). Formalin-fixed, paraffin-embedded tissue from the orbitofrontal cortex of each case was trimmed and cut into 6- μm sections using a microtome. Slides were dry oven-baked for 20 min at 60°C followed by deparaffinization with fresh xylene and dehydration with sequential ethanol dilutions in water (100%, 95%, 75%, 50%). Endogenous peroxidase was inactivated by RNAscope Hydrogen Peroxide Solution (Advanced Cell Diagnostics, 322335) and antigen target retrieval was achieved by heating the samples in RNAscope Target Retrieval reagent (Advanced Cell Diagnostics, 322000) at 100°C for 30 min before the sections were pretreated with RNAscope Protease Plus (Advanced Cell Diagnostics, 322331) at 40°C for 30 min. Sections were then hybridized with Human G3BP1 RNAscope Probes (Advanced Cell Diagnostics, 567861) at 40°C for 2 h and the resulting signals were amplified and developed with RNAscope 2.5 HD Detection Kit-Red (Advanced Cell Diagnostics, 322360) according to the manufacturer's instructions. After hybridization, sections were washed with PBS-TX (PBS, 0.15% TritonTM X-100) and blocked with 4% normal donkey serum in PBS-TX at room temperature for 1 h. Blocked sections were incubated with TDP-43 antibody (1:1000, Proteintech, 10782-2-AP) at 4°C overnight. After 3×5 -min washes in PBS-T, secondary incubation was performed at ambient temperature with donkey α -rabbit 488 Alexa Fluor secondary antibody (1:500, Invitrogen, A-21206). Finally, slides were washed 3×5 min with PBS-TX and once with 0.1 M phosphate buffer pH 7.4 (0.08 M sodium phosphate dibasic and 0.02 M sodium phosphate monobasic) before coverslipping with ProLongTM Gold antifade reagent with 4',6-diamidino-2-phenylindole (DAPI) (Invitrogen, P36931).

Micrograph acquisition and quantification

Fluorescence micrographs of orbitofrontal cortex sections from ALS without FTLD ($n = 4$) and ALS/FTLD ($n = 4$) were captured using a Leica DMI6000B microscope with a $100\times$ objective lens on the Velocity Acquisition Suite (v.6.3, Perkin Elmer). For each section, a two-dimensional z-stack projection was produced from 25 micrographs captured at a depth of 0.25 μm through the z-axis. To allow for the quantification of G3BP1-positive mRNA granules (magenta channel) in each neuron with or without TDP-43 pathology (green channel), the green channel intensity was sufficiently enhanced to reveal cell boundaries. The number of G3BP1-positive mRNA granules were quantified from 25 randomly selected neurons demonstrating normal nuclear TDP-43 in the orbitofrontal cortex of ALS without FTLD ($n = 4$) and ALS/FTLD-TDP-43 ($n = 4$) (100 neurons total from each condition). The same

sampling strategy was used resulting in the quantification of G3BP1-positive mRNA granules from an additional 100 neurons demonstrating TDP-43 pathology in ALS/FTLD-TDP-43 cases ($n = 4$). Statistical analysis comparing the mean number of G3BP1-positive mRNA granules in neurons with normal nuclear TDP-43 in ALS without FTLD-TDP-43 pathology and ALS/FTLD-TDP-43 versus neurons with nuclear depletion and cytoplasmic TDP-43 aggregation in ALS/FTLD-TDP-43) was performed using paired one-way ANOVA ($P < 0.0001$).

RNA-sequencing analysis

The RNA-sequencing (RNA-seq) data from human frontal cortex and cerebellum³⁹ (GEO accession: GSM1642314; SRA study: SRP056477) were downloaded and run in a bioinformatics pipeline using the Compute Canada clusters. Alignment was performed using HISAT2⁴⁰ against reference genome Hg38. Read counts were obtained with HTSeq-count⁴¹ and differential expression analysis was performed with the Bioconductor R package DESeq2.⁴² Data were normalized using DESeq2's median of ratios method. Polyadenylation site usage in human lumbar spinal motor neurons⁴³ (GEO accession: GSE103225; SRA study: SRP116386) was determined with QAPA.⁴⁴

Statistics

Data were graphed and analysed using Prism v.6.00 (GraphPad Software). Statistical tests are stated in the figure legends. Data were compared via two-tailed paired and unpaired *t*-tests, Mann-Whitney, one-way and two-way ANOVA with statistical significance established at $P < 0.05$.

Data availability

The data that support the findings of this study are available from the corresponding author, on reasonable request.

Results

TDP-43 nuclear depletion and disease-associated TDP-43 variants decrease G3BP1 levels

We have previously demonstrated that depletion of TDP-43 results in a downregulation of G3BP1 protein levels.¹⁶ As ALS/FTLD cases predominantly display a cytoplasmic mislocalization of TDP-43 concomitant with its nuclear depletion, we investigated whether cytoplasmic-restricted TDP-43 could rescue G3BP1 protein levels. To this end, we expressed an siRNA-resistant cDNA encoding TDP-43 with an inactivated nuclear localization signal (FLAG-TDP-43^{ANLS}) following siRNA-mediated depletion of endogenous TDP-43 in HeLa cells. Immunofluorescence analysis confirmed the cytoplasmic expression of the exogenous construct FLAG-TDP-43^{ANLS} in comparison to mock transfected control cells (Supplementary Fig. 1A and B), as previously reported.²⁴ Expression of FLAG-tagged TDP-43^{ANLS} in the context of endogenous TDP-43 depletion yielded a ~50% decrease in G3BP1 protein levels (siCTL + mock versus siTDP-43 + TDP-43^{ANLS}, $P = 0.0029$) comparable to G3BP1 levels in TDP-43 siRNA treated cells cotransfected with empty plasmid (Fig. 1A and B). Thus, cytoplasmic-restricted TDP-43 does not rescue G3BP1 protein levels.

Overexpression studies of TDP-43 ALS-associated mutations have reported defects in stress granule disassembly and/or cytoplasmic aggregation.^{10,45} However, this is a phenotype frequently observed in studies involving the overexpression of aggregation prone RBPs. Thus, we opted to evaluate the impact of a familial ALS-causing mutation (N352S) genome edited onto both

endogenous TDP-43 alleles in SH-SY5Y cells.⁴⁶ Consistent with Melamed et al.,⁴⁶ we noted a 30% decrease in TDP-43 protein levels ($P = 0.0334$), which correlated with a 30% reduction in G3BP1 protein levels (Fig. 1C and D; $P = 0.0393$). This reduction was also recapitulated at the mRNA level (Supplementary Fig. 1D; $P = 0.0413$). In addition, expression of TDP-35, an N-terminal truncated TDP-43 variant generated via alternative transcriptional start codon usage that is used more often in ALS patients and is predominantly localized in cytoplasmic granules,⁴⁷ also compromised G3BP1 protein levels (Fig. 1E, F and Supplementary Fig. 1C; $P = 0.0065$). Here, we also noted that endogenous TDP-43 levels were reduced 40% ($P = 0.0489$). Thus, expression of two pathological TDP-43 variants, which are associated with decreased endogenous TDP-43 levels, resulted in reduced G3BP1 protein.

TDP-43 uniquely modulates one of two protein-encoding G3BP1 transcripts

According to the Genotype-Tissue Expression (GTEx) project, two transcripts encode the same G3BP1 protein (ENT00000394123.7 and ENST00000356245.7), the former of which has only recently been annotated. The two transcripts primarily differ in the size of their 3' UTRs (8901 versus 1466 nt), hereafter called the long and short G3BP1 transcript, with the first 1466 nt being shared between the two isoforms (Fig. 2A). Using primer pairs to the distal 3' end of the longer transcript, we confirmed the presence of the longer 3' UTR-containing transcript to varying amounts in six different cell lines via qPCR with reverse transcription (RT-qPCR) (Fig. 2B).

Our previous work indicated that siRNA-mediated depletion of TDP-43 decreased G3BP1 mRNA levels,¹⁶ but these studies were performed using probe sets targeting exonic G3BP1 sequence, and therefore were unable to differentiate between long and short G3BP1 isoforms. To address the question of whether TDP-43 regulates one or both transcripts, we performed smFISH, a quantitative method to directly visualize and count transcripts. Specifically, we used smFISH probes against a shared sequence within both G3BP1 mRNA isoforms to target the total pool of G3BP1 transcripts versus probes against a unique region in the 3' UTR of the long G3BP1 transcript. This was performed on HeLa cells treated with control, G3BP1 and TDP-43 siRNA (Fig. 2C and Supplementary Fig. 2). Notably, the specificity of the smFISH probes was validated by the significant loss of signal in siG3BP1 cells compared to siControl (Fig. 2C and Supplementary Fig. 2A). In siControl, total G3BP1 foci were seen to be significantly more abundant than the long G3BP1 foci (5.7-fold), demonstrating that the long transcript is not the major G3BP1 mRNA isoform (Supplementary Fig. 2C). In corroboration, only ~13% of the total G3BP1 foci (magenta) counted co-localized with long G3BP1 foci (green) (Supplementary Fig. 2D). Interestingly, we observed a significant reduction (~2.7-fold, $P < 0.0001$) in the number of total G3BP1 foci in siTDP-43 cells compared to siControl, whereas no significant difference was found for the long G3BP1 foci (Fig. 2C and D). Moreover, we observed that ~75% of the long G3BP1 foci (green) co-localized with the total G3BP1 foci (magenta) (Supplementary Fig. 2D). We expect that the 25% of non-co-localized foci account for false negatives/positives as well as the orientation of the transcript in the *z*-plane. Given these data, we can confidently extrapolate that the abundance of the short G3BP1 transcript can be represented by the long foci subtracted from the total foci count. Herein, we show the short G3BP1 transcript specifically to be significantly reduced (~3.7-fold) as a consequence of reduced TDP-43 levels ($P < 0.0001$; Fig. 2D). We further confirmed this result in several cell lines by separately assessing total and long G3BP1 isoforms via RT-qPCR. Downregulation of TDP-43 using siRNA in HeLa, SK-N-SH and SH-SY5Y lowered total G3BP1 levels (HeLa: $P = 0.0222$; SK-N-SH: $P = 0.0067$; SH-SY5Y:

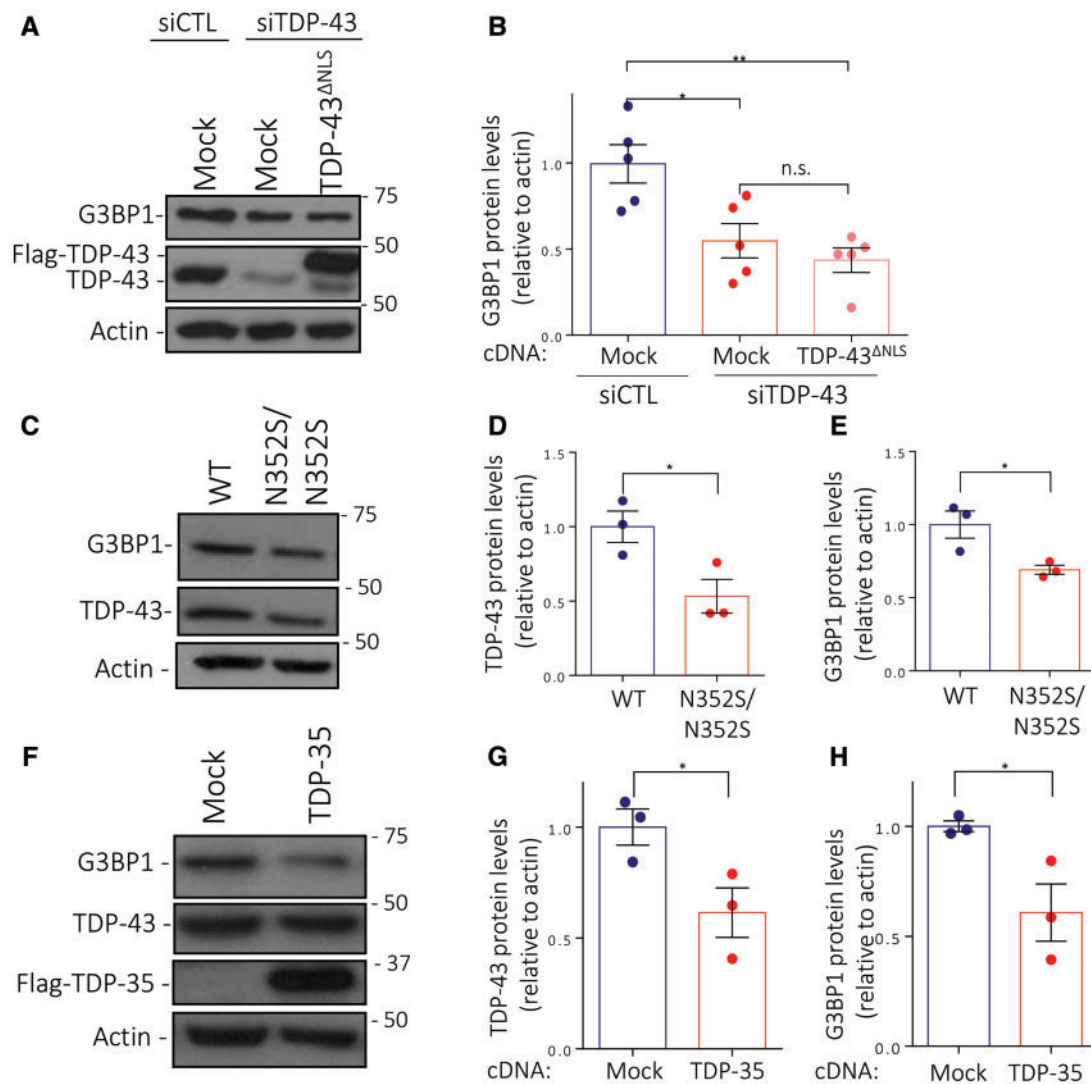


Figure 1 TDP-43 nuclear depletion and ALS-related species induce G3BP1 downregulation. (A) HeLa cells were transfected with siTDP-43 or siControl (siCTL), then transfected with empty plasmid (Mock) or Flag-TDP-43^{ΔNLS} and immunoblotted. (B) Quantification via densitometry of G3BP1 protein levels normalized to actin. (C) Protein from SH-SY5Y wild-type and TDP-43^{N352S/N352S} cells were extracted, and immunoblotted. Quantification via densitometry of (D) TDP-43 and (E) G3BP1 protein levels normalized to actin. (F) HeLa cells were transfected with empty plasmid (Mock) or Flag-tagged TDP-35 and immunoblotted. Quantification via densitometry of (G) TDP-43 and (H) G3BP1 protein levels normalized to actin. Data from three to five independent experiments are expressed as the mean fold change \pm SEM; Unpaired t-test * $P < 0.05$; ** $P < 0.01$. WT = wild-type.

$P = 0.0271$, consistent with our previous results^{16,18} (Fig. 2E). However, using a probe set to uniquely identify G3BP1 long transcripts, we found that the longer isoform was not significantly affected by TDP-43 knockdown in all three cell types tested (Fig. 2F and G). Collectively, these data indicate that it is the shorter G3BP1 transcript that is modulated by TDP-43.

TDP-43 stabilizes the short G3BP1 isoform via its 3' UTR

Since TDP-43 depletion is associated with a downregulation of the short G3BP1 transcript, we first sought to determine whether this was mediated by the promoter or the 3' UTR. Using a reporter assay in which the promoter and short 3' UTR were each fused to an optimized *Renilla* reporter gene (RenSP), siRNA-mediated depletion of TDP-43 reduced steady state luciferase activity of the G3BP1 3' UTR construct by 44% compared to control (GAPDH, Fig. 3A, $P = 0.036$). In contrast, the luciferase activity of the G3BP1 promoter reporter was not significantly changed compared to controls (Supplementary Fig. 3). The abundance of mRNA is frequently

governed by 3' UTR elements linked to mRNA stability. To evaluate whether TDP-43 stabilizes G3BP1 mRNA, we used a doxycycline-repressible transcript containing His-tagged G3BP1 cDNA fused to the short G3BP1 3' UTR. This approach allowed us to specifically determine exogenous G3BP1 mRNA decay without altering total cellular metabolism (as is observed with Actinomycin D treatment).⁴⁸ In TDP-43-depleted conditions, the exogenous G3BP1 transcript was 4-fold less stable than in siControl treated cells ($t_{1/2}$ siCTL: 4.1 ± 0.4 h versus $t_{1/2}$ siTDP-43: 1.4 ± 0.1 h, $P = 0.0031$; Fig. 3B and C). Thus, TDP-43 is required to stabilize the short G3BP1 transcript.

The 3' UTR of G3BP1 harbours a highly conserved UG-rich regulatory element

TDP-43 preferentially binds UG-rich sequences,^{3,49} which are often associated with mRNA stability.^{50,51} To better characterize TDP-43-dependent stabilization of G3BP1, we analysed the human short 3' UTR using RBPmap, which predicts RBP binding sites.⁵² A cluster of 13 potential TDP-43 binding sites were identified, located within nt

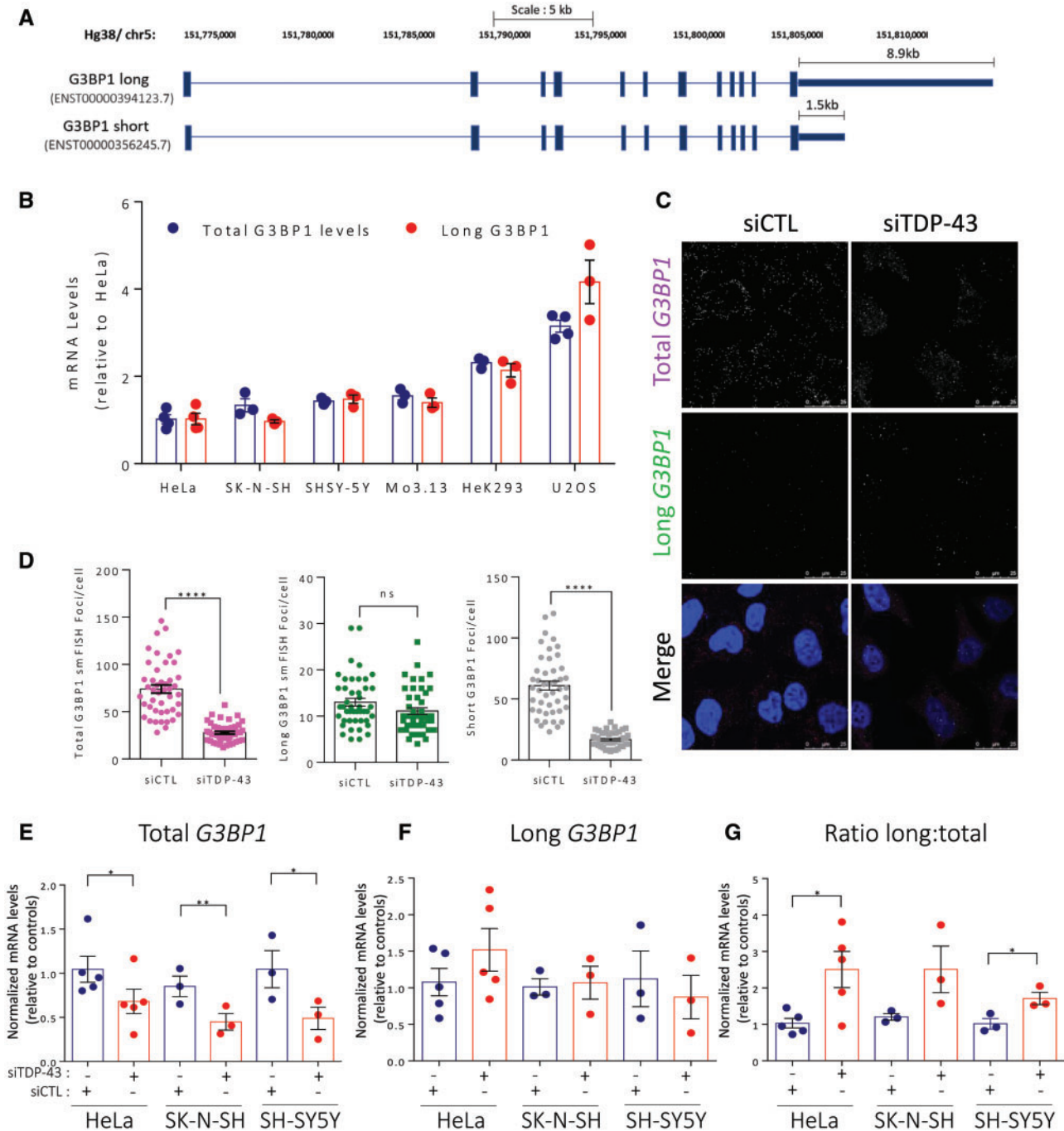


Figure 2 TDP-43 depletion only affects the short G3BP1 transcript. (A) Schematic of Genome Reference Consortium Human GRCh38.p12 G3BP1 transcripts. Long transcript has 8901-nt 3' UTR while the shorter version has a 1466-nt 3' UTR. (B) RT-qPCR for total G3BP1, long G3BP1 transcripts and GAPDH of extracted RNA from HeLa, HEK293, SK-N-SH, SH-SY5Y, U2OS and Mo3.13 cells, normalized with GAPDH and 18S, $n = 3-4$. (C) Representative images of smFISH in HeLa cells treated with siControl and siTDP-43, using probes against total G3BP1 (magenta) and long G3BP1 (green) mRNA. Cell nuclei were counterstained with Hoechst. Yellow foci show co-localization of total and long signal. (D) Total G3BP1 and long G3BP1 were quantified and short G3BP1 was calculated as the number of long foci subtracted from total magenta foci for each cell. Data are expressed as the mean \pm SEM, $n = 3$, $N = 45$. Unpaired t-test, **** $P < 0.0001$, scale bar = 25 μ m. (E and F) RT-qPCR for total G3BP1 and long G3BP1 transcripts extracted RNA from HeLa, SK-N-SH and SH-SY5Y cells transfected with siControl or siTDP-43 and normalized with GAPDH and 18S. (G) Ratio of the levels of long G3BP1 transcripts:total G3BP1, mean \pm SEM, $n = 3-5$, unpaired t-test * $P < 0.05$, ** $P < 0.01$.

334–358 of the 3' UTR of both transcripts (GRCh38/hg38 chr5:151 804 220–151 804 244; Fig. 4A). Nucleotide alignment of this sequence across 13 different species indicated an element at 3' UTR^{nt341-357} (GRCh38/hg38 chr5: 151 804 227–151 804 243) that is highly conserved across all species examined despite overall degeneration of the 3' UTR between species (Supplementary Table 3).

MEME analysis⁵³ confirms the conservation of UG repeats in this 16-nt element (Fig. 4B). TDP-43 and its orthologues are structurally conserved throughout evolution, especially within the RBD.⁴⁹ Moreover, G3BP1 is also conserved in *C. elegans*, with only one protein-encoding transcript, corresponding to the shorter isoform. Consistent with our data in human cell lines, *tdp-1* null worms⁵⁴

exhibit a 2-fold decrease of *gtbp-1* (G3BP1 orthologue) mRNA compared to N2 control worms (Fig 4C; $P = 0.0246$). Thus, G3BP1 mRNA contains a highly conserved UG-rich cis regulatory element in its 3' UTR that is functionally regulated by TDP-43.

TDP-43 stabilizes G3BP1 mRNA via a conserved 3' UTR regulatory element

To investigate the relevance of the identified conserved sequence, we revisited the luciferase reporter assay using a construct where a region including the regulatory element was deleted (G3BP1 3' UTR^{A319-372}; Fig 4D). Unlike the intact short G3BP1 3' UTR, or the positive control HDAC6, siRNA-mediated depletion of TDP-43 had no effect on the steady state luciferase activity of G3BP1 3' UTR^{A319-372} (Fig 4E). Moreover, using a doxycycline-repressible version of this construct with only the 16-nt conserved element deleted (G3BP1 3' UTR^{A341-357}; Fig 4D), we determined that the half-life of this exogenous transcript was comparable in the presence and absence of TDP-43 (4.6 ± 1.7 h versus 3.9 ± 0.8 h, $P = 0.58$; Fig 4F and G). The data obtained here indicate that the identified 16-nt UG-rich regulatory element is required for TDP-43-mediated stabilization of the short G3BP1 transcript.

TDP-43 directly binds the conserved element with high affinity

To determine whether TDP-43 mediates stabilization of G3BP1 mRNA via binding to the transcript, we performed immunoprecipitation of endogenous TDP-43 followed by RT-PCR of associated mRNAs. G3BP1 transcripts, including the long transcript, were recovered from TDP-43 immunoprecipitates, as was the positive control CAMKII⁵⁵ suggesting that other factors such as other RNA-binding proteins or a structural feature may also influence the regulation. HSPA1A served as a negative control⁵⁵ (Fig 5A). Next, to determine whether the stabilizing effect of TDP-43 on the short G3BP1 transcript was due to binding to the identified conserved element, we performed an RNA pull-down. Using a biotinylated probe (G3BP1 3' UTR^{nt319-372}) and HeLa whole cell extracts, we retrieved TDP-43 from the lysate, similar to a probe derived from GRN, which has been previously reported to be bound by TDP-43⁵⁶ (Fig 4B). The binding was considered specific since an AC-rich probe [(AC)₁₂] was not bound by endogenous TDP-43 but was by hnRNP L, an RBP with a preference for AC-rich sequences.⁵⁷ To determine whether the interaction between the 3' UTR regulatory

element of G3BP1 and TDP-43 was direct, the RNA pull-down was repeated using commercially produced recombinant TDP-43 protein. Both the G3BP1 and GRN probes, but not the (AC)₁₂ probe, were bound by recombinant TDP-43 (rTDP-43) (Fig 5B). Thus, TDP-43 directly binds the region containing the conserved regulatory element in the 3' UTR of G3BP1.

To establish that the binding was via the RBD of TDP-43 and to determine the affinity of the interaction of TDP-43 for the 3' UTR element, we performed an *in vitro* EMSA using highly purified components. The RBD of TDP-43 (TDP-43₁₀₂₋₂₆₉) efficiently bound a 32-nt RNA encompassing the G3BP1 3' UTR conserved regulatory sequence (G3BP1-RNA₃₂) and corresponding to G3BP1 3' UTR^{nt340-378}. This binding was accompanied by formation of two main shifted bands on the gel, as observed in previous binding studies with (TG)₁₂ DNA oligomers.⁵⁸ Given that the G3BP1-RNA₃₂ contains two GUGUGU sequences that have the potential to serve as independent binding sites, we speculate that these two bands represent the formation of RNA-protein complexes containing either one or two molecules of TDP-43₁₀₂₋₂₆₉. Interestingly, the wild-type TDP-43₁₀₂₋₂₆₉ binds with very high affinity to G3BP1-RNA₃₂. In contrast, there is no evidence of RNA binding for the TDP-43₁₀₂₋₂₆₉ protein fragment containing mutations that inactivate the RNA-binding pocket (F147L/F149L) at concentrations up to 1 μ M (Fig 5C and D). EMSA experiments performed in multiple replicates with the wild-type TDP-43₁₀₂₋₂₆₉ indicate an average K_d value of 3.1 ± 0.4 nM. Thus, taken together, these data demonstrate a high affinity of TDP-43 for the identified conserved element in the short 3' UTR of G3BP1.

Injury-induced TDP-43 nuclear efflux correlates with reduced G3BP1 in motor neurons *in vivo*

TDP-43 nuclear efflux has been reported in motor neurons of mice subjected to axotomy or permanent ligation.^{37,59} Thus, as a way to evaluate whether TDP-43 nuclear depletion can impact G3BP1 *in vivo*, we axotomized C57Bl/6 mice by severing the sciatic nerve just past the sciatic notch, as it exits the pelvic bone (Fig 6A). The behavioural evaluation of all injured mice was performed using the previously published NBA scoring system.^{37,38} At Day 1, axotomized mice exhibited notable paralysis of the foot with dragging, knuckle walking and no toe extension on the injured side (Fig 6B). This phenotype attenuated in the following days post-injury as shown by the significant decrease in the NBA score at Day 7 post-injury (Fig 6B). We confirmed the presence of axotomized motor neurons on the ipsilateral, but not the contralateral, side of the

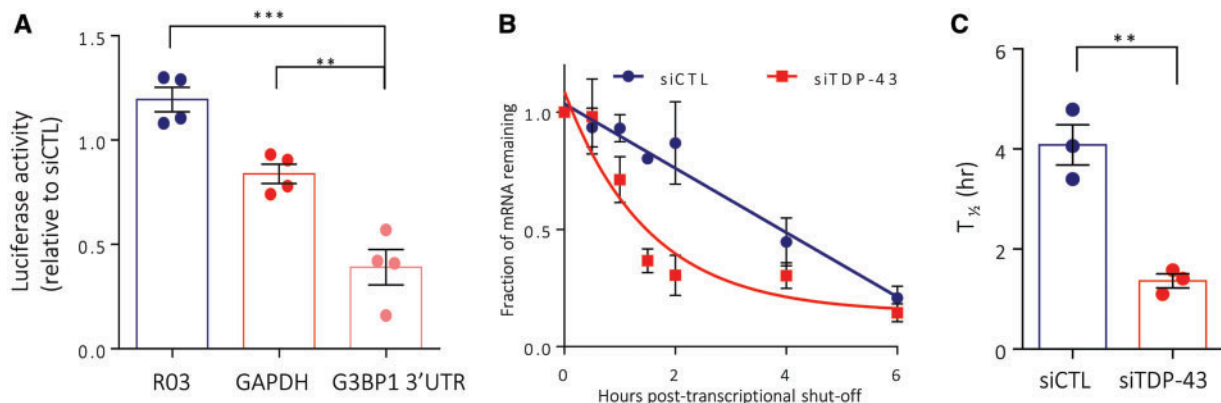


Figure 3 TDP-43 regulates and stabilizes G3BP1 via its 3' UTR. (A) HeLa cells were transfected with siTDP-43 or siCTL, then cotransfected with the indicated reporter plasmids. Luciferase activity of G3BP1 3' UTR is expressed relative to siCTL cells. GAPDH and R03 (random sequences) are used as controls, mean \pm SEM, $n = 4$, unpaired t-test $^{**}P < 0.01$, $^{***}P < 0.001$. (B) RT-qPCR for His-G3BP1 transcripts, normalized to 18S following doxycycline treatment for 6 h to shut off expression, $n = 3$. (C) Half-lives of His-G3BP1 transcripts in HeLa-Tet-off cells transfected with siCTL compared to cells transfected with siTDP-43, $n = 3$, unpaired t-test $^{**}P < 0.01$.

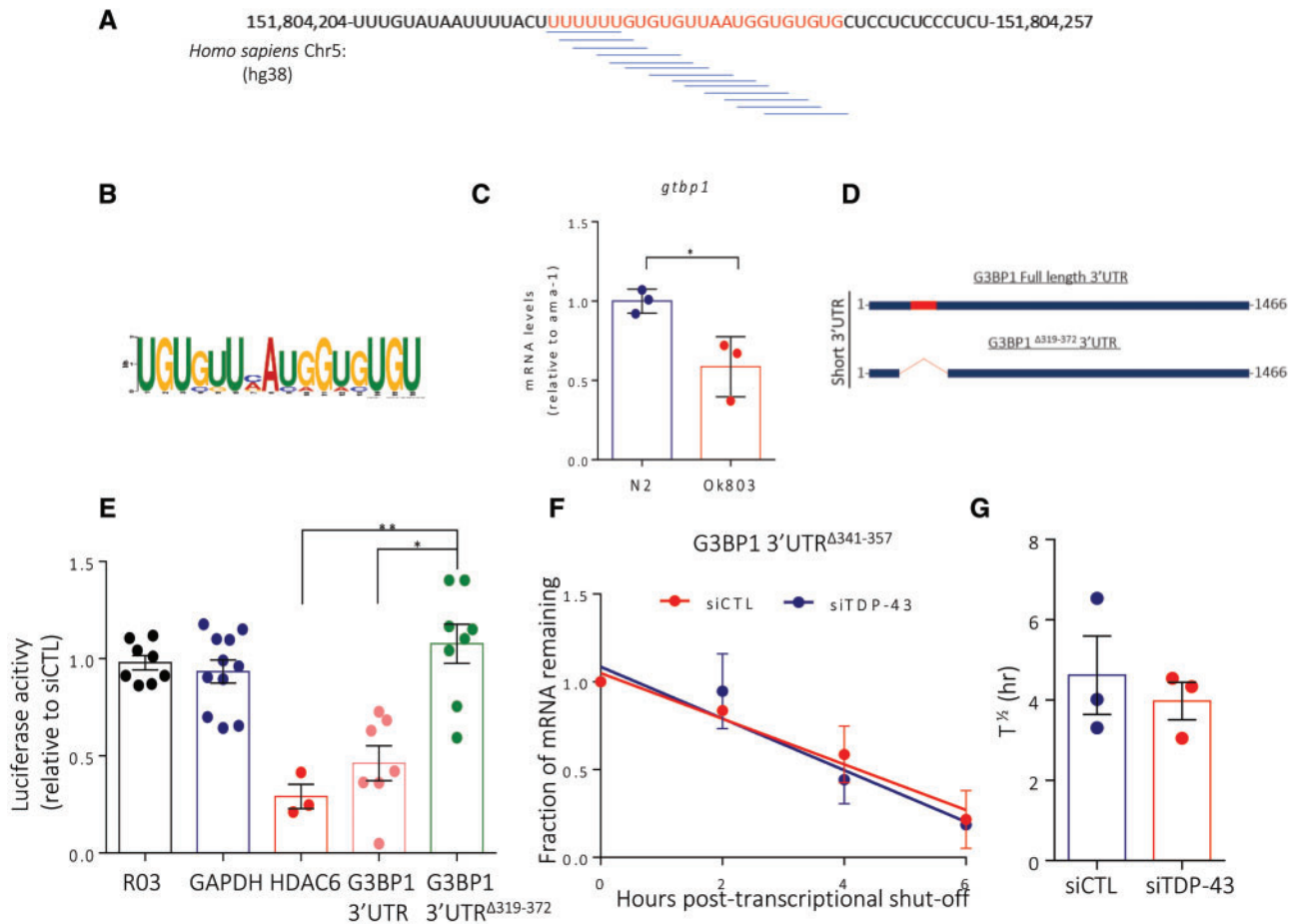


Figure 4 Identification of a conserved element in the G3BP1 3' UTR. (A) Schematic representation of the conserved element identified in the human G3BP1 3' UTR between nt 319 and 372 (GRCh38/hg38 chr5:151 183 766–151 183 816). The blue lines represent TDP-43 binding sites suggested by RNAmap. (B) Consensus sequence of the conserved sequence obtained from 13 species using the consensus sequence generator MEME. (C) RT-qPCR for *gtbp-1* of extracted RNA from N2 (wild-type control) and *tdp-1(ok803)* null worms. $n = 3$, unpaired t-test $*P < 0.05$. (D) Schematic representation of the G3BP1 3' UTR constructs used. The red rectangle represents the conserved element. (E) HeLa cells were transfected with siTDP-43 or siCTL, then cotransfected with the indicated reporter plasmids. GAPDH and R03 (random sequences) are negative controls and HDAC6 is a positive control, mean \pm SEM, $n = 3$ –8, unpaired t-test $*P < 0.05$, $**P < 0.01$. (F) RT-qPCR for His-G3BP1 ^{Δ 341–357} transcript, normalized to 18S following doxycycline treatment for 6 h to shut off expression. (G) Half-life of His-G3BP1 ^{Δ 341–357} transcript in HeLa-Tet-off cells transfected with siCTL compared to cells transfected with siTDP-43, $n = 3$.

ventral spinal cord using FluoroGold retrograde labelling (Fig. 6C). Investigation of TDP-43 expression/localization in injured neurons labelled with FluoroGold revealed 80% depletion of nuclear TDP-43 at Day 7 post-injury consistent with previous reports.^{37,59} This was accompanied by 70% reduction in G3BP1 expression in these motor neurons compared to the contralateral side (Fig. 6C and D; $P < 0.0001$). To verify the specificity of these observations, we also immunolabelled for FUS (Supplementary Fig. 4). After injury, FUS remained localized to the nucleus even at Day 7, consistent with previous work indicating that FUS is not regulated by TDP-43.^{16,18} Taken together, these results demonstrate an *in vivo* correlation between nuclear TDP-43 depletion and G3BP1 reduction in adult motor neurons.

The short G3BP1 transcript predominates in affected cell types and is reduced in ALS and ALS/FTD neurons

Given that only one of the two G3BP1 transcripts is sensitive to TDP-43 levels, it was imperative to determine the relative abundance of each transcript in cells/tissue of relevance to disease.

Analysis of published transcriptomics data from two different brain regions of healthy individuals³⁹ revealed a paucity of reads corresponding to the extended 3' UTR region of the long G3BP1 transcript in the frontal cortex, compared to the cerebellum (Fig. 7A), suggesting that the short G3BP1 transcript predominates in the frontal cortex. Analysis of global expression of G3BP1 (i.e. both transcripts) revealed a modest reduction in G3BP1 expression in the frontal cortex compared to the cerebellum, which demonstrated high variability across individuals (Fig. 7B; \log_2 FC = 0.30; $P = 0.04$). We also examined polyadenylation site usage in published transcriptomics data generated from lumbar spinal motor neurons isolated by laser capture microdissection from healthy individuals.⁴³ This analysis clearly indicated the preferential use of the proximal polyadenylation site, reflecting that the short G3BP1 transcript is more abundant than the longer isoform in the most ALS-vulnerable neurons (Fig. 7C; $P = 0.0004$). Both of these aforementioned datasets also included ALS and/or ALS/FTD cases. However, we were unable to detect a significant difference between G3BP1 3' UTR usage between controls and individuals with ALS or ALS/FTD, presumably due to the relatively low overall abundance of G3BP1 transcripts (data not shown). (Note, this dataset

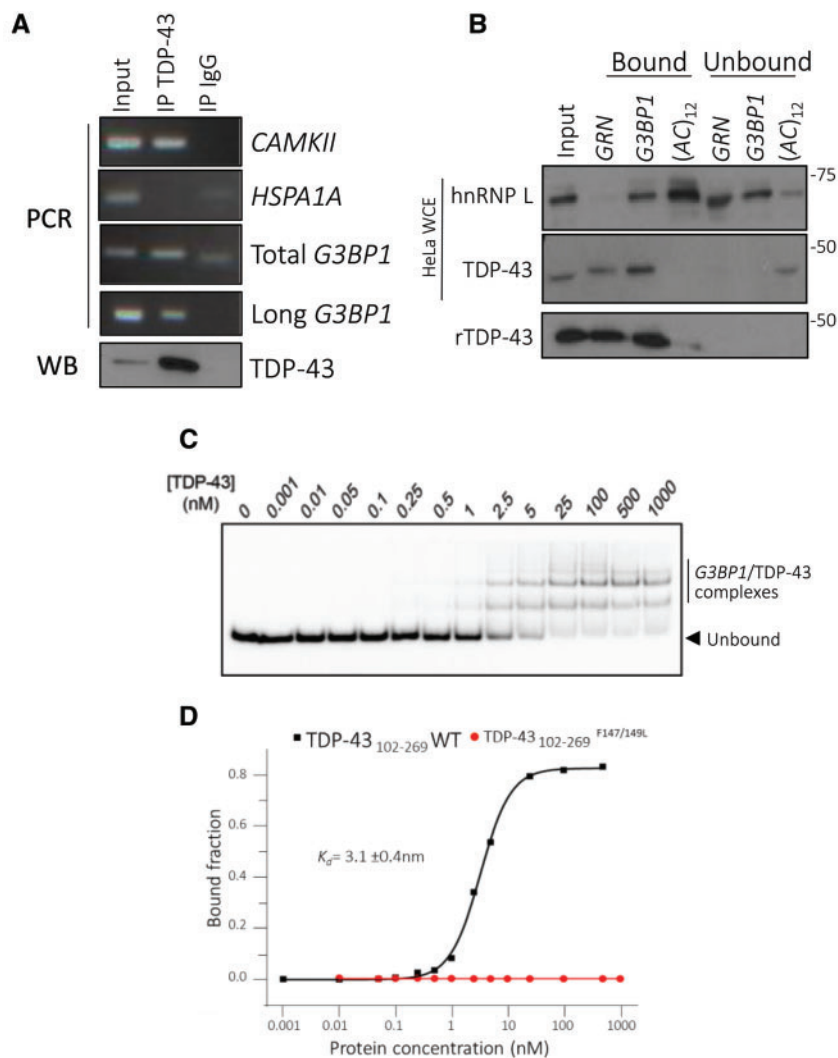


Figure 5 TDP-43 directly binds the conserved element. (A) TDP-43 protein and its associated transcripts were co-immunoprecipitated from HeLa cells homogenates. mRNAs binding to TDP-43 were extracted, reverse transcribed and amplified for *G3BP1* transcripts, *CaMKII* (positive control) and *HSPA1A* (negative control), showing that TDP-43 binds total *G3BP1* transcripts and the longer transcripts. Flag-immunoprecipitation serves as a control to demonstrate specificity of TDP-43 immunoprecipitation. (B) Proteins from whole HeLa cell extracts or TDP-43 recombinant protein (rTDP-43) were pulled down using biotinylated RNA probes containing the TDP-43 binding sequence in GRN (positive control), *G3BP1* 3' UTR^{nt319-372}, or (AC)₁₂ (negative control). For AC-repeat binding, hnRNP L served as a positive control. (C) Typical EMSA performed with 10 pM 5'-³²P-labelled RNA and increasing concentrations of TDP-43₁₀₂₋₂₆₉. (D) Typical binding curve using wild-type TDP-43₁₀₂₋₂₆₉ (black line) and the F147L/F149L mutant of TDP-43₁₀₂₋₂₆₉ (red line). IP = immunoprecipitation; WB = western blot; WCE = whole-cell extract; WT = wild-type.

had an average depth of only ~28 million reads per sample, and neither study implemented a strategy to enrich for low-abundance transcripts.) Thus, we assessed *G3BP1* transcript levels in human neurons differentiated from iPSCs via Ngn1-2 expression to yield a near-homogenous population of iPSC-derived neurons with properties consistent with glutamatergic, excitatory forebrain-like neurons (i³Neurons).^{28,29,60} These i³Neurons were modified to express a single copy of wild-type or mutant (M337V) TDP-43. Via RT-qPCR, we observed that *G3BP1* total transcript levels, but not the long transcript, were reduced 49% in TDP-43^{M337V} expressing i³Neurons compared to wild-type TDP-43 i³Neurons (Fig. 7D; $P = 0.0272$). In agreement with our data, this result indicates that it is the shorter *G3BP1* transcript impacted by the TDP-43 mutation.

Finally, to directly quantify total *G3BP1* transcripts in the context of TDP-43 pathology, we performed quantitative *in situ* hybridization using RNAscope probes to *G3BP1* coupled with

immunofluorescence labelling using TDP-43 antibody on orbitofrontal cortices of ALS/FTLD cases with cortical TDP-43 pathology in comparison with ALS cases without FTLD and no cortical TDP-43 pathology ($n = 4$ each; Supplementary Table 2). The number of *G3BP1* transcripts detected using RNAscope was equivalent in cortical neurons with normal nuclear TDP-43 localization (Fig. 7E) in both ALS/FTLD-TDP-43 cases and ALS/no FTLD cases (14.1 ± 3 and 14.4 ± 4 , respectively, $n = 100$ neurons per group; Fig. 7F). In contrast, *G3BP1* transcript levels were reduced 60% in ALS/FTLD neurons with TDP-43 pathology (5.9 ± 2.5 puncta per neuron; $n = 100$ neurons, $P = 2.5 \times 10^{-35}$; Fig. 7E and F), as evidenced by nuclear depletion and cytoplasmic mislocalization of TDP-43 (Fig. 7E, arrows). Taken together, these data are consistent with the concept that *G3BP1* mRNA is destabilized in the absence of nuclear TDP-43 in disease-affected neurons in ALS/FTLD.

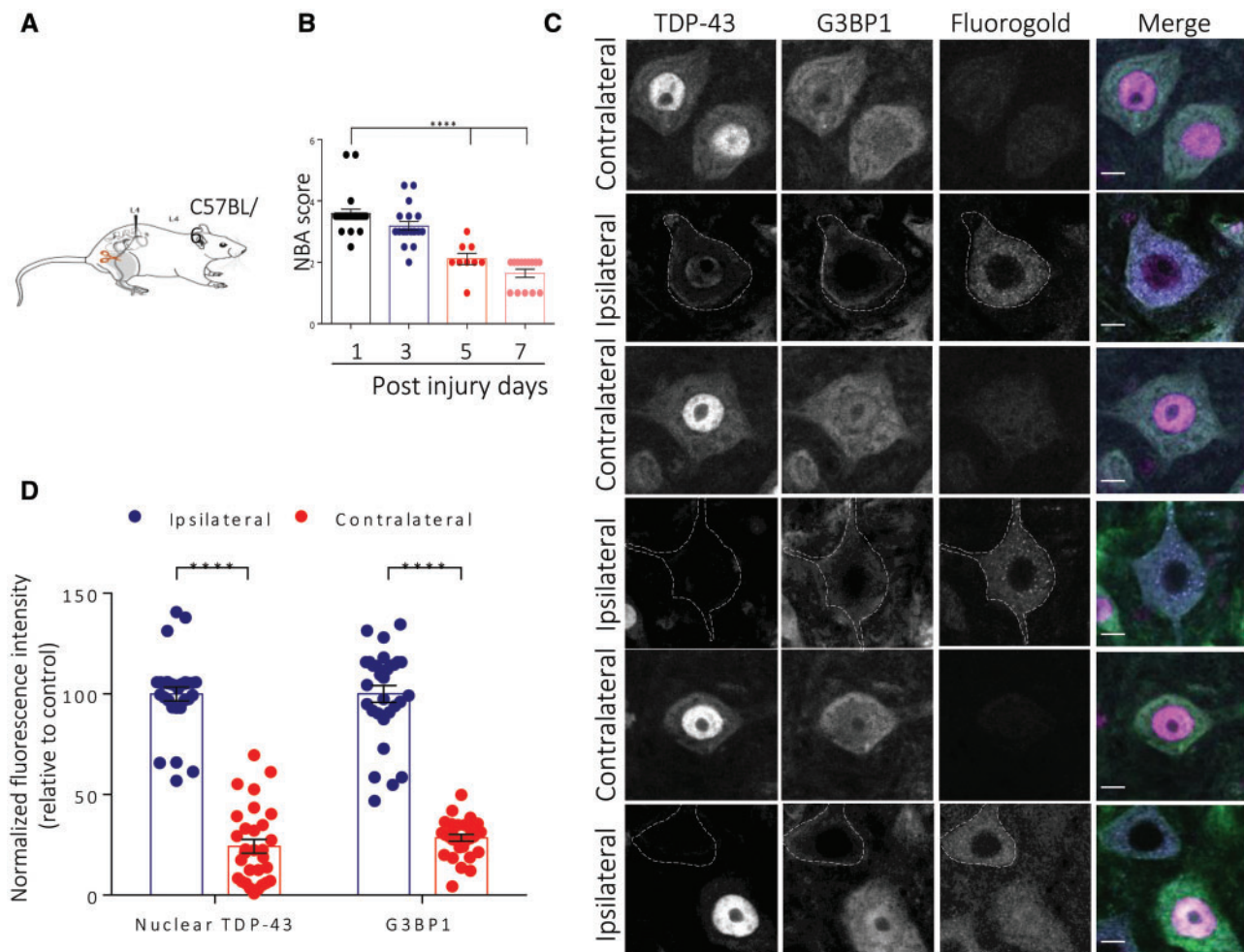


Figure 6 Changes in TDP-43 and G3BP1 expression in injured motor neurons following medial axotomy. (A) Schematic of the medial site of axotomy. (B) NBA score of the axotomized mice at Days 1, 3, 5 and 7. Data are expressed as the mean \pm SEM; Unpaired t-test **** P < 0.0001. (C) Representative images of control non-axotomized (ipsilateral) and axotomized mice (contralateral) spinal cord tissues at Day 7, showing injured spinal motor neurons of the ventral horn using mouse TDP-43, rabbit G3BP1 and guinea pig FluoroGold antibody. The grey line shows the cell boundary. (D) Fluorescence intensity of nuclear TDP-43 and total G3BP1 for the control non-injured and injured motor neurons at Day 7, $n = 3$ mice and $N = 10$ cells per mouse. Data are expressed as the mean \pm SEM; two-way ANOVA **** P < 0.0001. Scale bar = 10 μ m.

Discussion

In this study, we demonstrate the mechanism by which the loss of TDP-43 leads to reduced levels of G3BP1 mRNA and protein.^{16–18} We found that TDP-43 binds to and regulates the G3BP1 short transcript via its 3' UTR, similar to that described for HDAC6, ADD2 and MAPT.^{50,51,56,61} TDP-43 depletion reduces the stability of the most abundant G3BP1 transcript, explaining the observed decrease in G3BP1 protein level in TDP-43-depleted cells. In general, cellular stress and pathology are associated with an increase in the proportion of shorter transcripts, suggesting that this TDP-43 regulated transcript may become elevated in adverse conditions^{62–64} and thus outcompete the longer transcript for translation. Moreover, short and long 3' UTRs can be differentially regulated with long 3' UTR transcripts generally being longer-lived.⁶⁵ Several factors including RNA structure, RNA modifications and competitive/collaborative binding with other RBPs or miRNAs can affect translatability and localization of a given transcript. As TDP-43 binds both transcripts, it is possible that these other factors are key elements to differential G3BP1 transcript stability and warrant further investigation.

We propose that the mechanism by which TDP-43 stabilizes the short G3BP1 transcript is by binding the nascent transcript in the nucleus prior to its export across the nuclear membrane and protecting it from cytoplasmic mRNA decay. This is akin to HuR-mediated mRNA stability, which binds transcripts in the nucleus and protects them from TTP-mediated decay.⁶⁶ Our smFISH data indicate that the long G3BP1 mRNA has a higher ratio of nuclear transcripts than the short G3BP1 mRNA (Supplementary Fig. 2E). Thus, one possibility is that the long transcript is not susceptible to siTDP-43 mediated instability as less of the transcript is present in the cytoplasm, where mRNA decay mainly occurs, compared to the short G3BP1 transcript. However, as mentioned before, further study is required to fully evaluate the mechanisms that could account for differential G3BP1 transcript stability.

In the context of ALS/FTD, TDP-43 is typically found to be cytoplasmic, and thus in theory should be able to stabilize G3BP1 transcripts in the cytoplasm. However, consistent with our data, it is plausible that nuclear TDP-43 depletion as observed in patients with ALS means that TDP-43 is not available to nascent G3BP1 transcripts in the nucleus as they are transcribed, and thus these transcripts are not protected from mRNA decay on transfer to

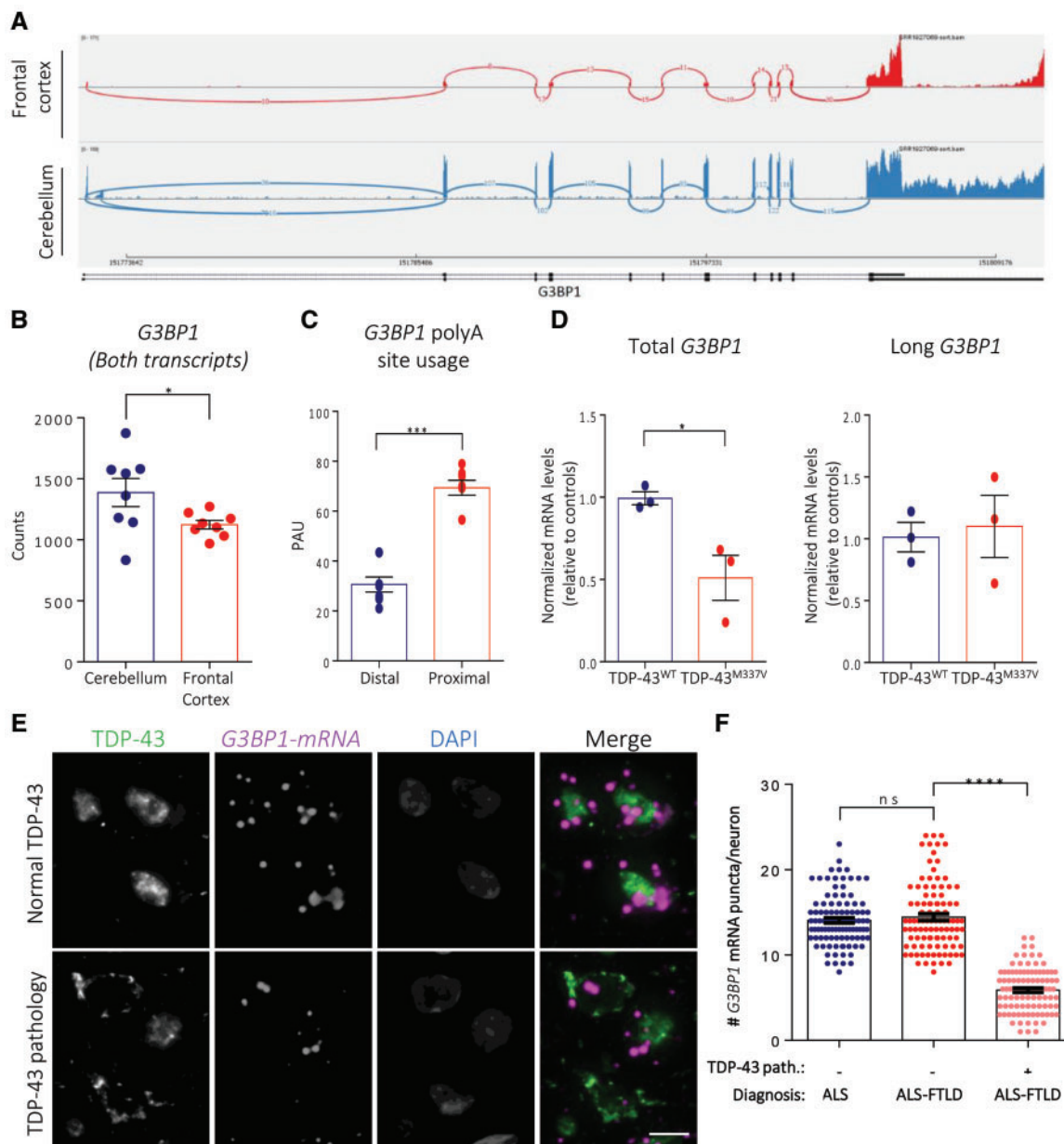


Figure 7 G3BP1 short mRNA is destabilized and reduced in patients with TDP-43-mediated neurodegeneration. (A) Sashimi plots of GEO dataset GSE67196 for human G3BP1 in cerebellum and frontal cortex of control case, showing reduced reads for the long G3BP1 3' UTR in the frontal cortex. (B) Comparison of G3BP1 levels (both transcripts) in human cerebellum and frontal cortex in healthy controls. * $P < 0.05$. (C) Quantification of polyadenylation site usage in G3BP1 transcripts in lumbar spinal motor neurons isolated by laser capture microdissection (GEO dataset GSE103225). Data are expressed as the mean \pm SEM; unpaired t-test **** $P < 0.001$. (D) RT-qPCR for total G3BP1 and long G3BP1 transcripts extracted RNA from I3 neurons derived from TDP-43^{M337V} and isogenic control fibroblast, mean \pm SEM, $n = 3$, paired t-test * $P < 0.05$. Normalized to GAPDH and 18S. (E) Neurons in the orbitofrontal cortex of ALS and ALS/FTLD cases showing normal nuclear localization of TDP-43 (top row, green) or nuclear TDP-43 depletion/cytoplasmic TDP-43 accumulation (bottom row, green). G3BP1 mRNA (magenta dots) is labelled with RNAscope probes, nuclei are marked with DAPI (blue). (F) Quantification of G3BP1 mRNA signals in neurons of the orbitofrontal cortex of ALS and ALS/FTLD with or without TDP-43 pathology (defined as obvious cytoplasmic accumulations or reduced nuclear TDP-43 levels). Data are expressed as the mean \pm SEM; one-way ANOVA **** $P < 0.0001$. Scale bar = 10 μ m.

cytoplasm. Another consideration is that cytoplasmic TDP-43 as detected in post-mortem samples is typically in an aggregated state, phosphorylated and insoluble, i.e. it is in a conformational state that precludes its normal physiological function. This is supported by Mann *et al.*⁶⁷ who used optogenetics to demonstrate that light-induced TDP-43 aggregates are phosphorylated, insoluble and can be reversed by RNA binding. Moreover, RNA is absent from these TDP-43 aggregates. Perhaps most compelling is that the authors also showed that RNA is not detected in phospho-TDP-43 inclusions in ALS spinal cord neurons or FTL

hippocampal neurons.⁶⁷ Taken together, this supports the model that cytoplasmic aggregated TDP-43 is not in a conformational state that can bind mRNA and thus would not be expected to co-localize with or stabilize G3BP1 mRNA in this compartment.

TDP-43 stabilizes G3BP1 transcripts via an evolutionary conserved cis regulatory sequence located within the 3' UTR. In alignment with recent findings of the ENCODE project, the identified regulatory element is UG-rich but not a pure UG cluster.⁶⁸ TDP-43 directly binds the regulatory element with a K_d that is 6–23 \times higher than that reported for small UG-rich RNAs (20–70 nM),⁴⁹ but

is similar to that reported for a 16-nt (2.8 nM)² and a 30-nt RNA (5 nM)² consisting entirely of UG repeats. While the entire G3BP1 3' UTR sequence is poorly conserved among the 13 species examined (and 10 additional species, data not shown), the 16-nt element we identified is very highly conserved and functional, as supported by our data in *C. elegans* where the sequence is 67% conserved. Together, these findings indicate that the regulatory element is necessary and sufficient for TDP-43 mediated stabilization of G3BP1 mRNA. Interestingly, the conserved element we have identified lies within a region that harbours very few single nucleotide polymorphisms (SNPs) (UCSC genome browser, VarSome), which demonstrates a conservation of the sequence and possibly indicates that deviation from this sequence is poorly tolerated. The few SNPs observed were initially predicted to be pathogenic and all increase or decrease the number of UG in the sequence, although they are currently classified as uncertain (VarSome). Further work will be needed to define whether any of these SNPs can be exploited to inform on disease onset or progression. Taken together, our data reinforce the evolutionary importance of TDP-43-mediated regulation of G3BP1, and by extension, its cellular function.

Transcriptomics data indicate that G3BP1 is expressed at relatively low levels in neurons (GTEX) and this could suggest that it is subject to very fine/tight regulation. However, our experience with mouse spinal cord shows that motor neurons are the major cell type in which G3BP1 signal is detected (Fig. 6 and unpublished data). We show that the short 3' UTR G3BP1 transcript is the predominant one expressed in disease-vulnerable frontal cortex and lumbar spinal motor neurons and G3BP1 mRNA levels were reduced in ALS/FTLD neurons bearing TDP-43 cytoplasmic inclusions/nuclear clearance. Our data in axotomized motor neurons, where loss of nuclear TDP-43 positively correlated with a sharp decrease in total G3BP1 levels are supportive of this possibility. Finally, near-physiological expression of ALS-associated TDP-43 mutations had the same impact on G3BP1 levels as nuclear TDP-43 depletion suggesting that TDP-43 mutations can act through a loss of function mechanism.

G3BP1 is essential for neuronal homeostasis and survival.^{69–72} Indeed, G3BP1 genetic deletion in 129/*sv* mice results in widespread neuronal loss, while the same deletion on a *Balb/c* background yields synaptic and locomotor deficits, with 75% of homozygotes displaying paralysis of at least one limb.^{70,71} In addition, these mice have impairments in neuronal plasticity and in calcium/glutamate signalling.^{69,70} G3BP1 is also a known target of certain enteroviruses, such as poliovirus and coxsackievirus B3, which each encode a protease that cleaves G3BP1 and effectively cripples the stress granule response to facilitate virus replication in motor neurons.^{73–75} It is noteworthy that poliovirus exhibits tropism for ALS-vulnerable regions (i.e. it infects the anterior horns of the spinal cord, brainstem and the motor cortex but not the oculomotor nerve).^{74,76} As lytic viruses, they cause selective motor neuron death and, in the case of poliovirus, induce a progressive paralysis (post-poliomyelitis syndrome) similar to that experienced by patients with ALS.⁷⁷

Collectively, our data support that under normal conditions, TDP-43 functions to stabilize G3BP1 transcripts via a highly conserved cis 3' UTR regulatory element. In addition, we observed reduced G3BP1 mRNA levels in neurons bearing the TDP-43 pathological signature of ALS/FTLD. The loss of G3BP1 mRNA, and thus the encoded protein that is essential to stress granule assembly, would preclude the launch of the protective neuronal response known as stress granule formation and draws into question the model that TDP-43 inclusions derive from defective stress granule disassembly. As we have previously published that deficient stress granule assembly contributes to enhanced neuronal

vulnerability,^{16–18} our data are consistent with the idea that stabilization of G3BP1 mRNA and maintenance of stress granule dynamics could be a valid therapeutic avenue.

Acknowledgements

We thank Nathalie Arbour for access to the plate reader and Aurélie Cleret-Buhot of the CRCHUM Cytometry, Cell Imaging and Molecular Pathology platform for help with microscopy. We thank Don Cleveland, Tania Kastelic and Dominique Cheneval for important discussions; Sarah Peyrard for laboratory management, Srivathsan Adivarahan and Daniel Zenklusen for help with smFISH probe design and troubleshooting, and Julie Veriepe and Audrey Labarre for advice with *C. elegans* experiments. We also thank André Dagenais, Yves Berthiaume and Francis Migneault for providing the pTRE-Tight vector, Catherine Laroche for Mo3.13 cells and Marjorie Labrecque, Jay Ross and Patrick Dion for help with RNA-seq analysis. We thank present and past C.V.V. laboratory members for constructive and helpful feedback.

Funding

This work was supported by the ALS Canada/Brain Canada Hudson Translational Team Grant (C.V.V.), CIHR (J.A.P., J.R. and P.L.), the Muscular Dystrophy Association (C.V.V.), the James Hunter ALS Initiative (J.R., L.Z.), the ALS Association Milton Safenowitz Postdoctoral Fellowship (PMM) and the National Institutes of Health (National Institute for Neurological Disorders and Stroke) R01-NS097542 (S.J.B.), National Institute for Aging P30 AG053760 (S.J.B.), the University of Michigan Protein Folding Disease Initiative and Ann Arbor Active Against ALS (S.J.B.). H.S. is supported by an FRQS Doctoral Studentship. M.T., C.V.V. and J.A.P. are FRQS Research Scholars.

Competing interests

The authors report no competing interests.

Supplementary material

Supplementary material is available at *Brain* online.

References

1. Taylor JP, Brown RH Jr, Cleveland DW. Decoding ALS: From genes to mechanism. *Nature*. 2016;539(7628):197–206.
2. Kuo PH, Chiang CH, Wang YT, Doudeva LG, Yuan HS. The crystal structure of TDP-43 RRM1-DNA complex reveals the specific recognition for UG- and TG-rich nucleic acids. *Nucleic Acids Res*. 2014;42(7):4712–22.
3. Mompean M, Romano V, Pantoja-Uceda D, et al. The TDP-43 N-terminal domain structure at high resolution. *Febs J*. 2016; 283(7):1242–60.
4. Afroz T, Hock E-M, Ernst P, et al. Functional and dynamic polymerization of the ALS-linked protein TDP-43 antagonizes its pathologic aggregation. *Nat Commun*. 2017;8(1):45.
5. Neumann M, Sampathu DM, Kwong LK, et al. Ubiquitinated TDP-43 in frontotemporal lobar degeneration and amyotrophic lateral sclerosis. *Science*. 2006;314(5796):130–133.
6. Forman MS, Trojanowski JQ, Lee VMY. TDP-43: A novel neurodegenerative proteinopathy. *Curr Opin Neurobiol*. 2007;17(5): 548–555.

7. Al-Chalabi A, Hardiman O. The epidemiology of ALS: A conspiracy of genes, environment and time. *Nat Rev Neurol*. 2013;9(11):617–28.
8. Mackenzie IR, Nicholson AM, Sarkar M, et al. TIA1 mutations in amyotrophic lateral sclerosis and frontotemporal dementia promote phase separation and alter stress granule dynamics. *Neuron*. 2017;95(4):808–816.e9.
9. Boeynaems S, Bogaert E, Kovacs D, et al. Phase separation of C9orf72 dipeptide repeats perturbs stress granule dynamics. *Mol Cell*. 2017;65(6):1044–1055.e5.
10. Dewey CM, Cenik B, Sephton CF, et al. TDP-43 is directed to stress granules by sorbitol, a novel physiological osmotic and oxidative stressor. *Mol Cell Biol*. 2010;31(5):1098–1108.
11. Sidibé H, Vande Velde C. RNA granules and their role in neurodegenerative diseases. In: Oeffinger M, Zenklusen D, eds. *The biology of mRNA: structure and function*. Springer International Publishing; 2019:195–245.
12. Anderson P, Kedersha N. RNA granules. *J Cell Biol*. 2006;172(6):803–808.
13. Anderson P, Kedersha N. Stress granules: The Tao of RNA triage. *Trends Biochem Sci*. 2008;33(3):141–150.
14. Tourrière H, Chebli K, Zekri L, et al. The RasGAP-associated endoribonuclease G3BP assembles stress granules. *J Cell Biol*. 2003;160(6):823–831.
15. Humoud MN, Doyle N, Royall E, et al. Feline calicivirus infection disrupts assembly of cytoplasmic stress granules and induces G3BP1 cleavage. *J Virol*. 2016;90(14):6489–6501.
16. McDonald KK, Aulas A, Destroismaisons L, et al. TAR DNA-binding protein 43 (TDP-43) regulates stress granule dynamics via differential regulation of G3BP and TIA-1. *Hum Mol Genet*. 2011;20(7):1400–1410.
17. Aulas A, Caron G, Gkogkas CG, et al. G3BP1 promotes stress-induced RNA granule interactions to preserve polyadenylated mRNA. *J Cell Biol*. 2015;209(1):73–84.
18. Aulas A, Stabile S, Vande Velde C. Endogenous TDP-43, but not FUS, contributes to stress granule assembly via G3BP. *Mol Neurodegener*. 2012;7:54.
19. Khalifallah Y, Kuta R, Grasmuck C, Prat A, Durham HD, Vande Velde C. TDP-43 regulation of stress granule dynamics in neurodegenerative disease-relevant cell types. *Sci Rep*. 2018;8(1):7551.
20. Yang P, Mathieu C, Kolaitis R-M, et al. G3BP1 is a tunable switch that triggers phase separation to assemble stress granules. *Cell*. 2020;181(2):325–345.e28.
21. Sanders DW, Kedersha N, Lee DSW, et al. Competing protein-RNA interaction networks control multiphase intracellular organization. *Cell*. 2020;181(2):306–324.e28.
22. Guillén-Boixet J, Kopach A, Holehouse AS, et al. RNA-induced conformational switching and clustering of G3BP drive stress granule assembly by condensation. *Cell*. 2020;181(2):346–361.e17.
23. Kabashi E, Lin L, Tradewell ML, et al. Gain and loss of function of ALS-related mutations of TARDBP (TDP-43) cause motor deficits in vivo. *Hum Mol Genet*. 2010;19(4):671–683.
24. Winton MJ, Igaz LM, Wong MM, Kwong LK, Trojanowski JQ, Lee VM. Disturbance of nuclear and cytoplasmic TAR DNA-binding protein (TDP-43) induces disease-like redistribution, sequestration, and aggregate formation. *J Biol Chem*. 2008;283(19):13302–9.
25. Deshaies JE, Shkreta L, Moszczynski AJ, et al. TDP-43 regulates the alternative splicing of hnRNP A1 to yield an aggregation-prone variant in amyotrophic lateral sclerosis. *Brain*. 2018;141(5):1320–1333.
26. Tank EM, Figueroa-Romero C, Hinder LM, et al. Abnormal RNA stability in amyotrophic lateral sclerosis. *Nat Commun*. 2018;9(1):2845.
27. Yu J, Chau KF, Vodyanik MA, Jiang J, Jiang Y. Efficient feeder-free episomal reprogramming with small molecules. *PLoS ONE*. 2011;6(3):e17557.
28. Busskamp V, Lewis NE, Guye P, et al. Rapid neurogenesis through transcriptional activation in human stem cells. *Mol Syst Biol*. 2014;10:760.
29. Lam RS, Topfer FM, Wood PG, Busskamp V, Bamberg E. Functional maturation of human stem cell-derived neurons in long-term cultures. *PLoS ONE*. 2017;12(1):e0169506.
30. Fernandopulle MS, Prestil R, Grunseich C, Wang C, Gan L, Ward ME. Transcription factor-mediated differentiation of human iPSCs into neurons. *Curr Protoc Cell Biol*. 2018;79(1):e51.
31. Weskamp K, Tank EM, Miguez R, et al. Neuronal hyperexcitability drives TDP43 pathology by upregulating shortened TDP43 protein isoforms. 2019:648477.
32. Gerbini T, Funahashi R, Luo Y, et al. Transcription activator-like effector nuclease (TALEN)-mediated CLYBL targeting enables enhanced transgene expression and one-step generation of dual reporter human induced pluripotent stem cell (iPSC) and neural stem cell (NSC) lines. *PLoS ONE*. 2015;10(1):e0116032.
33. Rahman S, Zorca CE, Traboulsi T, et al. Single-cell profiling reveals that eRNA accumulation at enhancer-promoter loops is not required to sustain transcription. *Nucleic Acids Res*. 2017;45(6):3017–3030.
34. Bolte S, Cordelières FP. A guided tour into subcellular colocalization analysis in light microscopy. *J Microsc*. 2006;224(Pt 3):213–32.
35. Salvail-Lacoste A, Di Tomasso G, Piette BL, Legault P. Affinity purification of T7 RNA transcripts with homogeneous ends using ARiBo and CRISPR tags. *RNA (New York, NY)*. 2013;19(7):1003–1014.
36. Di Tomasso G, Lampron P, Dagenais P, Omichinski JG, Legault P. The ARiBo tag: A reliable tool for affinity purification of RNAs under native conditions. *Nucleic Acids Res*. 2011;39(3):e18–e18.
37. Moisse K, Volkening K, Leystra-Lantz C, Welch I, Hill T, Strong MJ. Divergent patterns of cytosolic TDP-43 and neuronal progranulin expression following axotomy: Implications for TDP-43 in the physiological response to neuronal injury. *Brain Res*. 2009;1249:202–211.
38. Rodriguez A, Perez-Gracia E, Espinosa JC, Pumarola M, Torres JM, Ferrer I. Increased expression of water channel aquaporin 1 and aquaporin 4 in Creutzfeldt-Jakob disease and in bovine spongiform encephalopathy-infected bovine-PrP transgenic mice. *Acta Neuropathol*. 2006;112(5):573–85.
39. Prudencio M, Belzil VV, Batra R, et al. Distinct brain transcriptome profiles in C9orf72-associated and sporadic ALS. *Nat Neurosci*. 2015;18(8):1175–82.
40. Kim D, Paggi JM, Park C, Bennett C, Salzberg SL. Graph-based genome alignment and genotyping with HISAT2 and HISAT-genotype. *Nat Biotechnol*. 2019;37(8):907–915.
41. Anders S, Pyl PT, Huber W. HTSeq—a Python framework to work with high-throughput sequencing data. *Bioinformatics*. 2015;31(2):166–9.
42. Love MI, Huber W, Anders S. Moderated estimation of fold change and dispersion for RNA-seq data with DESeq2. *Genome Biol*. 2014;15(12):550.
43. Krach F, Batra R, Wheeler EC, et al. Transcriptome-pathology correlation identifies interplay between TDP-43 and the expression of its kinase CK1E in sporadic ALS. *Acta Neuropathol*. 2018;136(3):405–423.

44. Ha KCH, Blencowe BJ, Morris Q. QAPA: A new method for the systematic analysis of alternative polyadenylation from RNA-seq data. *Genome Biol.* 2018;19(1):45.
45. Liu-Yesucevitz L, Bilgutay A, Zhang YJ, et al. Tar DNA binding protein-43 (TDP-43) associates with stress granules: Analysis of cultured cells and pathological brain tissue. *PLoS ONE.* 2010;5(10):e13250.
46. Melamed Z, Lopez-Erauskin J, Baughn MW, et al. Premature polyadenylation-mediated loss of stathmin-2 is a hallmark of TDP-43-dependent neurodegeneration. *Nature Neurosci.* 2019;22(2):180–190.
47. Xiao S, Sanelli T, Chiang H, et al. Low molecular weight species of TDP-43 generated by abnormal splicing form inclusions in amyotrophic lateral sclerosis and result in motor neuron death. *Acta Neuropathol.* 2015;130(1):49–61.
48. Baird T, Hogg J. Using tet-off cells and RNAi knockdown to assay mRNA decay. *Methods Mol Biol.* 2018;1720:161–173.
49. Lukavsky PJ, Daujotyte D, Tollervey JR, et al. Molecular basis of UG-rich RNA recognition by the human splicing factor TDP-43. *Nat Struct Mol Biol.* 2013;20(12):1443–9.
50. Gu J, Wu F, Xu W, et al. TDP-43 suppresses tau expression via promoting its mRNA instability. *Nucleic Acids Res.* 2017;45(10):6177–6193.
51. Fiesel FC, Voigt A, Weber SS, et al. Knockdown of transactive response DNA-binding protein (TDP-43) downregulates histone deacetylase 6. *EMBO J.* 2010;29(1):209–221.
52. Paz I, Kosti I, Ares M Jr, Cline M, Mandel-Gutfreund Y. RBPmap: A web server for mapping binding sites of RNA-binding proteins. *Nucleic Acids Res.* 2014;42(Web Server issue):W361–7.
53. Bailey TL, Boden M, Buske FA, et al. MEME SUITE: Tools for motif discovery and searching. *Nucleic Acids Res.* 2009;37(Web Server issue):W202–W208.
54. Vaccaro A, Tauffenberger A, Ash PE, Carlomagno Y, Petrucelli L, Parker JA. TDP-1/TDP-43 regulates stress signaling and age-dependent proteotoxicity in *Caenorhabditis elegans*. *PLoS Genet.* 2012;8(7):e1002806.
55. Wang IF, Wu LS, Chang HY, Shen CK. TDP-43, the signature protein of FTL-D-U, is a neuronal activity-responsive factor. *J Neurochem.* 2008;105(3):797–806.
56. Colombrita C, Onesto E, Megiorni F, et al. TDP-43 and FUS RNA-binding proteins bind distinct sets of cytoplasmic messenger RNAs and differently regulate their post-transcriptional fate in motoneuron-like cells. *J Biol Chem.* 2012;287(19):15635–47.
57. Hui J, Hung LH, Heiner M, et al. Intronic CA-repeat and CA-rich elements: A new class of regulators of mammalian alternative splicing. *EMBO J.* 2005;24(11):1988–1998.
58. Buratti E, Baralle FE. Characterization and functional implications of the RNA binding properties of nuclear factor TDP-43, a novel splicing regulator of CFTR exon 9. *J Biol Chem.* 2001;276(39):36337–36343.
59. Urushitani M, Ezzi SA, Julien JP. Therapeutic effects of immunization with mutant superoxide dismutase in mice models of amyotrophic lateral sclerosis. *Proc Natl Acad Sci U S A.* 2007;104(7):2495–2500.
60. Zhang Y, Pak C, Han Y, et al. Rapid single-step induction of functional neurons from human pluripotent stem cells. *Neuron.* 2013;78(5):785–98.
61. Costessi L, Porro F, Iaconcig A, Muro AF. TDP-43 regulates beta-adducin (Add2) transcript stability. *RNA Biol.* 2014;11(10):1280–90.
62. Romo L, Ashar-Patel A, Pfister E, Aronin N. Alterations in mRNA 3' UTR isoform abundance accompany gene expression changes in human Huntington's disease brains. *Cell Rep.* 2017;20(13):3057–3070.
63. Zheng D, Wang R, Ding Q, et al. Cellular stress alters 3'UTR landscape through alternative polyadenylation and isoform-specific degradation. *Nat Commun.* 2018;9(1):2268.
64. Lau AG, Irier HA, Gu J, et al. Distinct 3' UTRs differentially regulate activity-dependent translation of brain-derived neurotrophic factor (BDNF). *Proc Natl Acad Sci U S A.* 2010;107(36):15945–15950.
65. Tushev G, Glock C, Heumüller M, Biever A, Jovanovic M, Schuman EM. Alternative 3' UTRs modify the localization, regulatory potential, stability, and plasticity of mRNAs in neuronal compartments. *Neuron.* 2018;98(3):495–511.e6.
66. Fan XC, Steitz JA. Overexpression of HuR, a nuclear-cytoplasmic shuttling protein, increases the in vivo stability of ARE-containing mRNAs. *EMBO J.* 1998;17(12):3448–60.
67. Mann JR, Gleixner AM, Mauna JC, et al. RNA binding antagonizes neurotoxic phase transitions of TDP-43. *Neuron.* 2019;102(2):321–338.e8.
68. Van Nostrand EL, Freese P, Pratt GA, et al. A large-scale binding and functional map of human RNA-binding proteins. *Nature.* 2020;583(7818):711–719.
69. Martin S, Bellora N, González-Vallinas J, et al. Preferential binding of a stable G3BP ribonucleoprotein complex to intron-retaining transcripts in mouse brain and modulation of their expression in the cerebellum. *J Neurochem.* 2016;139(3):349–368.
70. Martin S, Zekri L, Metz A, et al. Deficiency of G3BP1, the stress granules assembly factor, results in abnormal synaptic plasticity and calcium homeostasis in neurons. *J Neurochem.* 2013;125(2):175–184.
71. Zekri L, Chebli K, Tourrière H, et al. Control of fetal growth and neonatal survival by the RasGAP-associated endoribonuclease G3BP. *Mol Cell Biol.* 2005;25(19):8703–8716.
72. Sahoo PK, Lee SJ, Jaiswal PB, et al. Axonal G3BP1 stress granule protein limits axonal mRNA translation and nerve regeneration. *Nat Commun.* 2018;9(1):3358–3358.
73. Lloyd RE. Enterovirus control of translation and RNA granule stress responses. *Viruses.* 2016;8(4):93–93.
74. White JP, Cardenas AM, Marissen WE, Lloyd RE. Inhibition of cytoplasmic mRNA stress granule formation by a viral proteinase. *Cell Host Microbe.* 2007;2(5):295–305.
75. Fung G, Ng CS, Zhang J, et al. Production of a dominant-negative fragment due to G3BP1 cleavage contributes to the disruption of mitochondria-associated protective stress granules during CVB3 infection. *PLoS ONE.* 2013;8(11):e79546.
76. Nagata N, Iwasaki T, Ami Y, et al. A poliomyelitis model through mucosal infection in transgenic mice bearing human poliovirus receptor, TgPVR21. *Virology.* 2004;321(1):87–100.
77. Xue YC, Feuer R, Cashman N, Luo H. Enteroviral infection: The forgotten link to amyotrophic lateral sclerosis? *Front Mol Neurosci.* 2018;11:63.